
Position: Many generalization measures for deep learning are fragile

Shuofeng Zhang¹ Ard A. Louis¹

Abstract

A wide variety of generalization measures have been applied to deep neural networks (DNNs). Although obtaining tight bounds remains challenging, such measures are often assumed to reproduce qualitative generalization trends. In this position paper, we argue that many post-mortem generalization measures—those computed on trained networks—are **fragile**: small training modifications that barely affect the underlying DNN can substantially change a measure’s value, trend, or scaling behavior. For example, minor hyperparameter changes, such as learning rate adjustments or switching between SGD variants can reverse the slope of a learning curve in widely used generalization measures like the path norm. We also identify subtler forms of fragility. For instance, the PAC-Bayes origin measure is regarded as one of the most reliable, and is indeed less sensitive to hyperparameter tweaks than many other measures. However, it completely fails to capture differences in data complexity across learning curves. This data fragility contrasts with the function-based marginal-likelihood PAC-Bayes bound, which does capture differences in data-complexity, including scaling behavior, in learning curves, but which is not a post-mortem measure. Beyond demonstrating that many bounds—such as path, spectral and Frobenius norms, flatness proxies, and deterministic PAC-Bayes surrogates—are fragile, this position paper also argues that developers of new measures should explicitly audit them for fragility.

1. Introduction

Classical generalization theories—based on VC dimension, Rademacher complexity and related tools—have a long his-

¹Rudolf Peierls Centre for Theoretical Physics, University of Oxford, United Kingdom. Correspondence to: Shuofeng Zhang <shuofeng.zhang@physics.ox.ac.uk>.

Code for this work can be found at https://github.com/shuofengzhang/Prior_bound

tory in machine learning. They were developed with two intertwined aims: to furnish tight mathematical guarantees and to explain generalization. For deep networks the same aspiration has driven a profusion of bounds. While tight bounds have proven elusive, with some exceptions (Dziugaite & Roy, 2017; Pérez-Ortiz et al., 2020; Valle-Pérez & Louis, 2020; Lotfi et al., 2022), the expectation has been that these measures can generate qualitative insight into the generalization behavior of deep neural networks (DNNs). These bounds have typically focused on weights after training, which is why they are sometimes called post-mortem bounds. Large-scale comparisons have compared the behavior of these measures, albeit often only at the sign level, e.g. does changing a setting produce the same a change in the underlying DNN and a generalization measure with the same sign (Jiang et al., 2019a; Dziugaite et al., 2020a).

A notable property of DNNs is that to first order, their generalization performance is robust to modest changes in network size, hyperparameters, optimisers, or stopping criteria. This raises a natural question: are generalization measures themselves equally robust to such changes? If a generalization measure captures the basic underlying factors that drive DNN performance, one would expect it to exhibit a similar degree of robustness.

The main finding of this paper is that many of the post-mortem bounds studied in the literature are *fragile*: small, ostensibly irrelevant training tweaks that barely affect the underlying DNN, can flip a measure’s shape, trend, or scale. To test these fragilities systematically, we evaluate measures under controlled perturbations that hold data and architecture, fixed while nudging a single training knob. Three stressors structure the audit in the main text: learning-curve behavior as sample size increases (§3); temporal behavior, including when the model has interpolated (§4); and responses to data complexity via label noise and dataset swaps (§5). In the supplementary material, we show more tests of fragility for a much wider set of measures.

In contrast to the post-mortem bounds, we show that a function-based marginal-likelihood PAC-Bayes bound successfully tracks dataset complexity and learning-curve scaling (Valle-Pérez & Louis, 2020). This bound is based on a simple measure of inductive bias, the probability that a random set of weights produces a function that fits the training

data set. Because it operates in function space and does not depend explicitly on training dynamics, this bound is inherently insensitive to the choice of optimiser or most training hyperparameters. This insensitivity is both a strength, making the bound robust rather than fragile, and a limitation, as it prevents the bound from reflecting how training procedures influence generalization, including effects such as feature learning. Nonetheless, the strong performance of this relatively simple approach suggests that developing more sophisticated function-space generalization measures could be a fruitful direction for future research.

Finally, we sketch a few potential causes of fragility, in the hope they can lead to new insights. We show that some of the qualitative failures of norm-based bounds with sample size appear to track a recent prediction of qualitative changes in the scaling of norms in the simpler setting of linear regression (Zhang & Louis, 2025). We also exploit a symmetry in scale-invariant networks and prove a non-asymptotic equivalence between fixed learning-rate with fixed weight decay and a matched run with exponentially increasing learning rate and time-varying weight decay; the two training procedures compute the same predictor at every iterate (§6; cf. Li & Arora, 2019). Under this invariance lever, magnitude-sensitive post-mortem measures can inflate by orders of magnitude while test error remains flat. This suggests that generalization measures should carefully track key invariances present in the underlying DNNs.

The widespread fragility we observe suggests that some generalization measures may be showing correlation in some limited settings that may not be related to causation. Our position is therefore not only that many measures are fragile, but also that investigators should carefully audit their measures for fragility, using the kinds of tests we propose in this paper.

Our contribution:

- We formulate a compact fragility audit for generalization measures that targets training-hyperparameter stability, post-interpolation temporal behavior, and data-complexity response.
- We provide systematic evidence that popular post-mortem measures—path, spectral and Frobenius norms, flatness proxies, and deterministic PAC–Bayes surrogates—change their qualitative predictions under mild optimiser or hyperparameter tweaks even when the underlying DNN accuracy is stable.
- We prove an equivalence for scale-invariant networks that matches fixed schedules to exponentially increasing learning-rate schedules with time-varying weight decay, yielding a controlled invariance lever that isolates function from parameter scale and exposes magnitude sensitivity.

2. Related work

We use *generalization bound* and *generalization measure* interchangeably: both seek to predict out-of-sample performance, differing mainly in whether they arrive with formal guarantees. In modern deep networks these quantities are best read as *measures*—diagnostics to compare across training/data regimes—rather than practically tight certificates.

From classical capacity to modern practice. Early theory framed capacity via VC and Rademacher analyses (Mendelson, 2002; Anthony & Bartlett, 2002; Bartlett & Mendelson, 2001; Koltchinskii, 2001). As overparameterization became the norm, evidence accumulated that uniform-convergence explanations often miss the mark: networks can fit random labels yet generalize on natural data (Zhang et al., 2016), some bounds fail to track risk (Nagarajan & Kolter, 2019), and benign overfitting can arise even at interpolation (Bartlett et al., 2020). The field responded with diagnostics that foreground invariances, algorithmic dependence, and data interactions.

2.1. Capacity-oriented diagnostics: norms, margins, distance from initialization

The first works in this subfield translated classical notions into deep settings. Spectrally-normalized margin bounds tied test error to Lipschitz-like control and margins, making scale explicit (Bartlett et al., 2017). Path- and norm-based views clarified how depth and weight scales shape effective complexity (Neyshabur et al., 2015; 2019). Empirically, modeling the *distribution* of margins—not just the minimum—improves predictiveness across trained families (Jiang et al., 2018; Novak et al., 2018), and sample complexity can depend on norms rather than width (Golowich et al., 2018). In practice, enforcing Lipschitz continuity often improves out-of-sample performance (Gouk et al., 2020; Yoshida & Miyato, 2017). Distance-from-initialization and movement-from-pretraining offer reference-aware, width-robust complexity surrogates with both empirical support and bounds (Li et al., 2018; Zhou et al., 2021; Neyshabur et al., 2017a), while optimization dynamics link large margins to implicit bias in separable regimes (Soudry et al., 2018).

2.2. Geometry-oriented diagnostics: flatness and sharpness

A parallel line approached generalization through loss-landscape geometry. The “flat minima generalize better” intuition predates deep learning (Hochreiter & Schmidhuber, 1997) and resurfaced when large-batch training was observed to converge to sharper minima with worse test error (Keskar et al., 2017). Because raw sharpness is parameterization-dependent, normalized and magnitude-

aware definitions were proposed and shown to correlate more robustly with test error (Dinh et al., 2017; Tsuzuku et al., 2020; Kim et al., 2022; Jang et al., 2022). These ideas also shaped algorithms: SAM explicitly optimizes a local worst-case neighborhood and typically improves accuracy; adaptive variants and ablations probe when and why it helps (Foret et al., 2020; Kwon et al., 2021; Andriushchenko & Flammarion, 2022). Independent probes—weight averaging, landscape visualizations, and training-dynamics analyses—add evidence that broader valleys often accompany better generalization (Izmailov et al., 2018; Li et al., 2017; Cohen et al., 2021). Stochastic optimization theory offers a mechanism: noise scale and heavy-tailed gradient noise can bias learning toward flatter regions (Smith et al., 2017; Jastrzebski et al., 2017; Simsekli et al., 2019; McCandlish et al., 2018).

2.3. Algorithm-aware certificates: PAC-Bayes as operational measures

Partly in response to limits of uniform convergence, PAC-Bayesian analysis made algorithm dependence explicit by trading empirical risk against a posterior–prior divergence (McAllester, 1999; Seeger, 2002; Catoni, 2007; Langford & Shawe-Taylor, 2002). The framework became operational when non-vacuous deep-network certificates were obtained by optimizing stochastic posteriors (Dziugaite & Roy, 2017), or simply working with the GP prior (Valle-Pérez et al., 2018; Zhang et al., 2021). Subsequent work tightened certificates with data-aware priors (Dziugaite, 2018; Pérez-Ortiz et al., 2020), and with compression-flavored posteriors that reduce effective description length (Arora et al., 2018a; Lotfi et al., 2022). Treating PAC-Bayes itself as a training objective yields models that are both accurate and tightly certified, while extensions broaden the scope to adversarial risk and fast/mixed-rate regimes (Rodríguez-Gálvez et al., 2024). However, one worry is that while these optimised measures may provide quantitatively tighter bounds, they do so at the expense of qualitative insight (Arora et al., 2018a).

Other perspectives. Complementary lenses provide boundary conditions any credible measure should respect. Algorithmic stability ties generalization to insensitivity under data perturbations (Bousquet & Elisseeff, 2002; Hardt et al., 2015); information-theoretic analyses bound excess risk by the information a learning rule extracts from the sample (Russo & Zou, 2016; Xu & Raginsky, 2017). Description-length and compression viewpoints link compressibility to generalization (Blier & Ollivier, 2018; Taiji Suzuki, 2020). Linearized regimes (NTK/GP) delineate when very wide nets behave like their kernel limits (Jacot et al., 2018; Lee et al., 2020b). Finally, double-descent phenomena and scaling laws offer external checks on diagnostics (Belkin et al., 2019; Kaplan et al., 2020).

Meta-evaluations and synthesis. Large-scale comparisons underscore that no single candidate explains generalization under all interventions (Jiang et al., 2019b; Dziugaite et al., 2020b), motivating a measures-as-diagnostics mindset. A recent critique shifts the lens from *predictiveness* to *tightness*, showing that uniformly tight bounds are out of reach in overparameterized settings and clarifying what such tightness could mean (Gastpar et al., 2023). Our focus is complementary: rather than tightness per se, we study *fragility*—how otherwise informative measures can fail under innocuous hyperparameter changes that leave underlying DNN performance essentially unchanged.

3. Training-hyperparameter fragility

The path norm (definition in App. A) is often regarded as the strongest norm-based proxy for modern ReLU networks: it respects layerwise rescalings and has supported some of the sharpest norm-style capacity statements and practical diagnostics (Neyshabur et al., 2015; 2017b; Gonon et al., 2023). Precisely because it is a strong candidate, it is a natural place to look for fragility.

In Fig. 1 we show a triptych for RESNET-50 on *FashionMNIST*, nudging exactly one hyperparameter at a time, either the optimizer or the learning rate (no early stopping), while keeping the data, model, and pipeline fixed. Each curve shows test error (black), the raw path norm (blue), and the path norm divided by the empirical margin (orange); axes are logarithmic and error bars reflect seed variability.

In the **left** plot, we run SGD with momentum at LR = 0.01: both path-norm curves start at a value of roughly ($\sim 10^5$) and decrease more or less log-linearly with increasing sample size, with the margin-normalized curve tracking about a decade lower. Both drop faster than the underlying RESNET-50 test error. Changing the optimizer to ADAM but keeping LR = 0.01 (**middle** panel) results in much smaller path norms (now near 10^{-1}) and striking non-monotonic behavior. A minor adjustment of ADAM’s learning rate to 0.001 (**right** panel)—and the metrics jump back up to $\sim 10^5$ – 10^6 but now collapse by four orders of magnitude as data size grows. These widely different behaviors arise purely from modest hyperparameter tweaks that barely affect the underlying RESNET-50 test error.

The contrasting behavior of the path-norm measure appears to mirror the simpler, analytically tractable case for linear regression. In that setting, for a fixed ℓ_r weight norm, qualitatively different scaling of the norm with sample size obtains depending on the ℓ_p -minimizer. More precisely, with $p \in [1, 2]$, the ℓ_r weight norm is monotonic in n if $r \leq 2(p-1)$ and plateaus if $r \leq 2(p-1)$ (Zhang & Louis, 2025). This implies that fixing *which* norm you measure does not fix its learning-curve scaling, because the solution

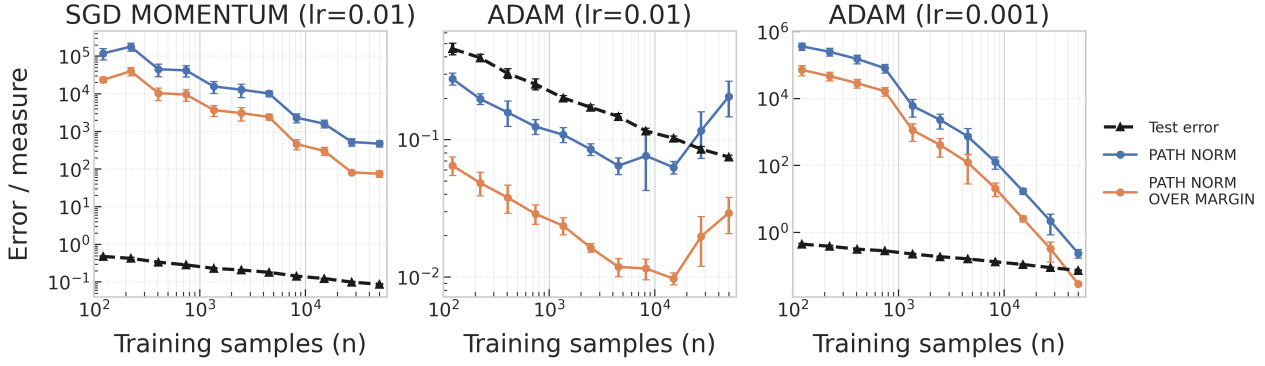


Figure 1. Path-norm learning curves under small training-pipeline changes (no early stopping). *Left:* SGD with momentum, LR = 0.01. *Middle:* ADAM, LR = 0.01. *Right:* ADAM, LR = 0.001. Curves show RESNET-50 test error (black), path norm (blue), and path norm over margin (orange); axes are logarithmic and error bars denote seed variability. Training set sizes n range from 10^2 to the full FashionMNIST training set (5×10^4 samples).

selected by optimization—through implicit (or explicit) bias, e.g., favoring different ℓ_p -minimizers—can induce different sample-size scalings of that same norm. This change in qualitative behavior was also illustrated in diagonal linear networks where the implicit bias can be tuned by varying the learning dynamics (Zhang & Louis, 2025). For the more complex setup of path-norm for RESNET-50 on FashionMNIST in Fig. 1, the optimizer and learning-rate choices may analogously shift the deep model’s implicit bias, toggling the path-norm scaling between monotone and U-shaped, just as was seen for linear regression and deep linear networks.

See App. A for precise definitions for the measures we consider as well as further experiments, including the same stress test across Frobenius, margin, spectral, PAC-Bayes, and VC-style proxies.

4. Temporal behavior fragility

Temporal traces ask a simple question that post-mortem snapshots cannot: once the classifier stops changing, does the measure stop moving? Let T_{int} denote the first epoch at which training accuracy reaches 100%. A stable diagnostic should largely settle for $t > T_{\text{int}}$; continued change indicates optimizer-driven drift rather than functional change.

A set of three experiments on FashionMNIST illustrates the point. We fix the architecture and data, then vary one knob at a time across the three panels of Figure 2. Holding the learning rate fixed at 0.01 and swapping the optimizer from SGD with momentum (left) to ADAM (middle) flips the post-interpolation regime: with SGD, the path norm sits near 5×10^2 and then slowly declines and the ratio-over-margin trends downward ($T_{\text{int}} \approx 27$), whereas with ADAM the path norm climbs from $\approx 10^{-2}$ to 10^0 and the ratio rises in step, continuing past interpolation ($T_{\text{int}} \approx 114$). Holding the optimizer fixed (ADAM) and re-

ducing the learning rate from 0.01 to 0.001 (right) again changes the temporal behavior: both traces drop rapidly and then increase moderately after the dashed line. In all cases, the generalization curve remains on a comparable scale.

A plausible mechanism underlies this split. After interpolation under cross-entropy, gradients can continue to increase logit scale along near-flat directions. ADAM tends to amplify this scale drift, while SGD+momentum tempers it, yielding opposite signs for the post-interpolation slope. The lesson is that weight-norm-based measures—and margin-normalized variants that co-move with them—are not monotone indicators of optimization progress: an upward trend can be optimizer-driven scale inflation; a flat or gently declining trend need not signal stagnation.

For practice, we recommend reporting T_{int} and the *post-interpolation slope* $s := \frac{d \log \text{Measure}}{d \log t} \Big|_{t > T_{\text{int}}}$ alongside any temporal plot; overlay optimizers on the same axes; and compare snapshots at matched milestones (e.g., the first 100%-accuracy crossing) or with early-stopped checkpoints. A useful stress test is *hysteresis*: resume a checkpoint taken just after T_{int} with a different optimizer and check whether the measure’s drift changes sign while test error holds steady. These checks make temporal fragility visible and keep optimizer-induced motion from being mistaken for learning. We refer the readers to Appendix B for experimental results on the temporal behaviors of more generalization measures.

5. Data-Complexity Fragility: Label Noise & Dataset Difficulty

How DNN performance varies with data complexity or sample size (learning curves) offers key insights into the mechanisms of generalization. Therefore, reporting how a generalization measure behaves under changes in data complexity

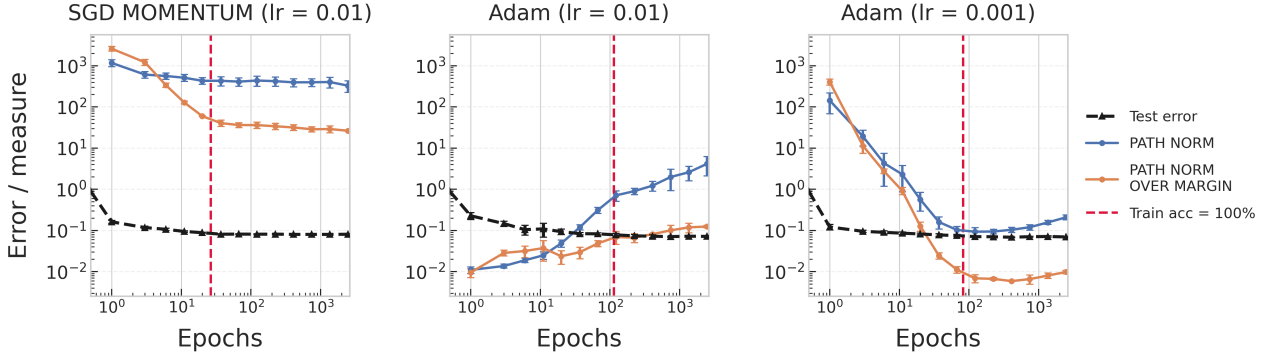


Figure 2. ResNet-50 on FashionMNIST as a function of training epochs. *Left* (SGD+momentum, LR = 0.01). *Middle* (ADAM, LR = 0.01). *Right* (ADAM, LR = 0.001). While the path norm and path norm over margin measures show qualitative different behavior upon small hyperparameter tweaks, the underlying generalization is similar across the three panels.

or sample size should be a standard part of its evaluation.

The first two panels in figure 3 illustrate how merely changing ADAM’s learning rate flips the qualitative trend of the path-norm curves (left vs. middle) with data complexity (for SGD with momentum on this data, see Appendix D). This illustrates the kind of fragility our framework urges authors to investigate and report when treating bounds as *measures*.

Finally, the last panel in figure 3 illustrates how the function-space ML-PACBayes measure provides a non-vacuous bound that tracks data-complexity (see also Appendix F). This performance is not mirrored by several PAC–Bayes *parameter-space* surrogates, which on the one hand are much less sensitive to training hyperparameters than the path norm measures are, but on the other hand exhibit a different more subtle kind of fragility; they are typically *insensitive* to label corruption in standard setups (see Appendix D). We call this behavior a fragility because it reflects a serious failing of these measures.

To illustrate data-complexity fragility, we chose the PACBAYES_ORIG measure (definition in App. A) because it is thought to be one of the best in its class. We hold the *architecture and hyperparameters fixed* and use the datasets MNIST, FASHIONMNIST, and CIFAR10. As illustrated in Figure 4, the dashed generalization–error curves separate cleanly and their *slopes* decrease with dataset difficulty (MNIST steepest decline, CIFAR-10 flattest). However, the first two panels of Figure 4 show that for a given set of hyperparameters, the PACBAYES_ORIG measure gives nearly identical numerical values for different datasets and therefore *fails to recognize changes in dataset complexity*: its learning-curve slopes are nearly indistinguishable across datasets and reflect changes in the test-error slopes. By contrast, the third panel (ML-PACBayes) is both *tight* (close to the corresponding error curves) and *data-aware*: it preserves the MNIST < FashionMNIST < CIFAR-10 ordering and reflects the different slopes. See Appendix F

for the bound’s definition and a fuller discussion of why this function-space quantity captures dataset difficulty while post-mortem parameter-space PAC-Bayes surrogates often do not.

There has been substantial recent interest in the study of scaling laws for deep neural networks (DNNs). These laws describe how generalization performance varies as a function of model size, training sample size, or computational cost (see, e.g., (Hestness et al., 2017; Kaplan et al., 2020; Spigler et al., 2019; Hoffmann et al., 2022; Valle-Pérez & Louis, 2020; Bahri et al., 2021; Nam et al., 2024; Goring et al., 2025) and references therein). Here, we observe that the ML-PACBayes bound does quite well at capturing the scaling behavior with the training sample size. However, it should be kept in mind that because this bound is evaluated with a Gaussian process (GP) method, it cannot capture feature-learning, which can play a crucial role in learning-curve scaling for certain datasets (Nam et al., 2024; Goring et al., 2025).

In App. G, we move beyond label corruption and dataset swaps, and also probe symmetry-preserving vs. signal-destroying data transforms via pixel permutations. Again, we find that the ML-PACBayes function-space predictor tracks the expected invariances while several post-mortem diagnostics do not.

6. Scale-invariant network and exponential learning rate schedule

Normalization layers make many modern networks effectively scale-invariant, and this symmetry underlies the “exponentially increasing learning-rate” idea of Li & Arora (2019): in such models, training with fixed learning rate (LR), weight decay (WD), and momentum can be matched—in function space—by a run with an exponentially increasing LR and *no* WD (plus a small momentum

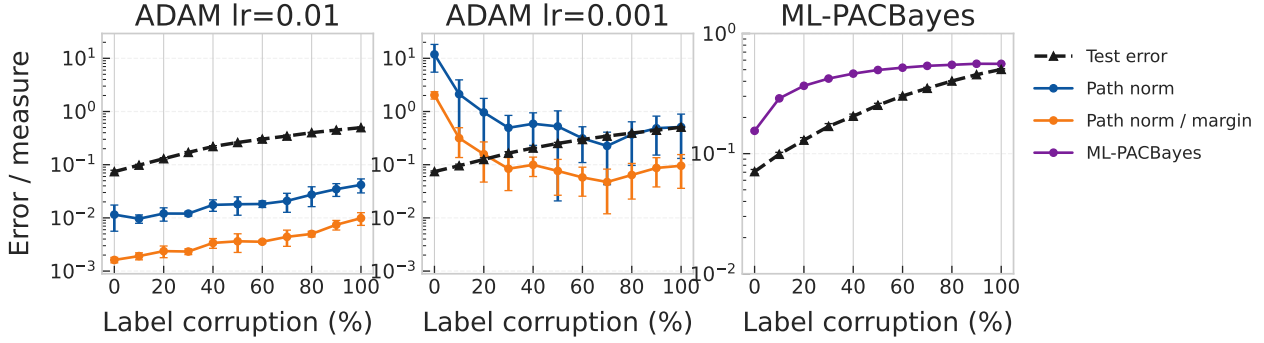


Figure 3. Label-corruption sweeps with post-mortem norms vs. function-space ML-PACBayes on RESNET-50. Left: ADAM, LR=0.01. Middle: ADAM, LR=0.001. Right: ML-PACBayes; purple, Dashed black: test error; blue: path norm; orange: path norm over margin. A ten-fold LR change reverses the path-norm trend (left vs. middle), while ML-PACBayes remains a smooth, monotone function of corruption (right) and is, by construction, agnostic to optimizer/LR. All panels use 10,000 training samples on binarized FashionMNIST.

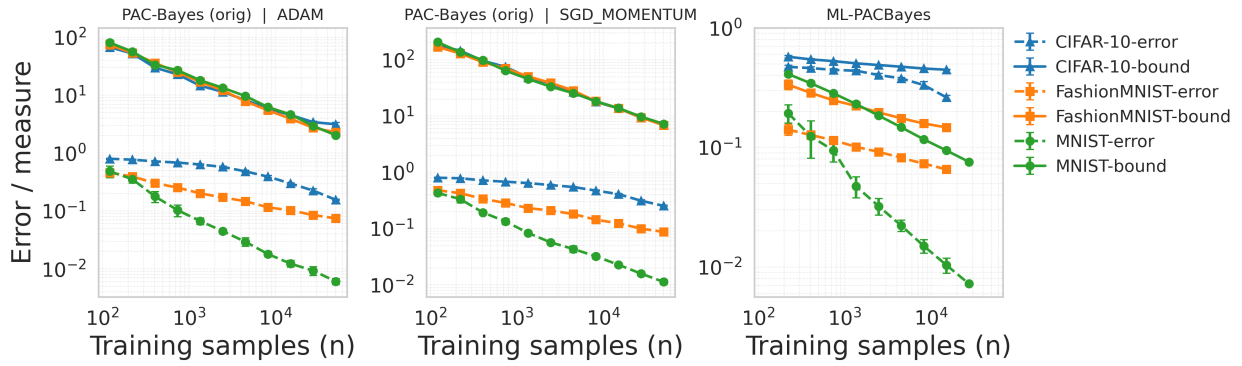


Figure 4. Fixed architecture, varying dataset.. The model is RESNET-50. Left: PACBAYES_ORIG with ADAM. Middle: PACBAYES_ORIG with SGD (momentum). Changing from ADAM to SGD with momentum leads to a small increase in the overall scale of the PACBAYES_ORIG learning curves (solid lines). However, for both optimisers, these learning curves don't distinguish MNIST, FASHIONMNIST, and CIFAR10, missing both the data-complexity ordering and the changing slopes visible in the underlying learning curves (dashed lines). Right: ML-PACBayes (marginal-likelihood PAC-Bayes) is tight and preserves the correct dataset ordering and reproduces the trends in the slope; for technical reasons, this panel is computed on the binarized versions of the three datasets.

correction across phases). Their analysis shows how LR and WD can be “folded into” an exponential schedule and documents successful experiments under this equivalence. We refer to this multiplicative control parameter α as the *Exp++ factor*.

We use the same symmetry but a different equivalence. Instead of removing WD, our theorem pairs an exponentially *increasing* LR with a *time-varying* WD so that every iterate computes the same predictor as a fixed-LR/fixed-WD baseline. The mapping is explicit and non-asymptotic: it gives closed-form schedules for $\tilde{\eta}_t$ and $\tilde{\lambda}_t$, and an admissible range for the multiplicative factor α via the interval \mathcal{I} . Conceptually, this creates a single “Exp++” knob that can drive large changes in parameter norms while leaving the learned function essentially unchanged—exactly the

benign intervention we later use to probe the fragility of magnitude-sensitive measures. Empirical details and results are deferred to Appendix H.

Definition 6.1 (Scale invariant neural networks). Consider a parameterized neural network $f(\theta)$. We say f is *scale invariant* if

$$\forall c \in \mathbb{R}^+, f(\theta) = f(c\theta) \quad (1)$$

Theorem 6.2 (Equivalence of schedules in scale-invariant nets). $(\text{GD+WD+LR fixed} \Leftrightarrow \text{GD+WD} \searrow + \text{LR} \nearrow)$. Let $f(\theta_t)$ be scale-invariant and let training use SGD with momentum γ . Introduce the shorthands

$$\Delta_\lambda := (1 - \gamma)^2 - 2(1 + \gamma)\lambda\eta_0 + (\lambda\eta_0)^2, \quad (2)$$

$$\Xi(\alpha) := \frac{\alpha^2 - \alpha(1 - \lambda\eta_0 + \gamma) + \gamma}{\eta_0}. \quad (3)$$

Define the interval endpoints

$$\alpha_L := \frac{\gamma}{1 - \lambda\eta_0 + \gamma}, \quad (4)$$

$$\alpha_- := \frac{1 + \gamma - \lambda\eta_0 - \sqrt{\Delta_\lambda}}{2}, \quad (5)$$

$$\alpha_+ := \frac{1 + \gamma - \lambda\eta_0 + \sqrt{\Delta_\lambda}}{2}, \quad (6)$$

and set

$$\mathcal{I} := (\alpha_L, \alpha_-] \cup [\alpha_+, 1). \quad (7)$$

Consider the two updates (with $\theta_{-1} = \theta_0$, $\tilde{\theta}_0 = \theta_0$, $\tilde{\theta}_{-1} = \alpha\theta_{-1}$):

$$\frac{\theta_t - \theta_{t-1}}{\eta_0} = \frac{\gamma(\theta_{t-1} - \theta_{t-2})}{\eta_0} - \nabla_\theta \left(L(\theta_{t-1}) + \frac{\lambda}{2} \|\theta_{t-1}\|_2^2 \right), \quad (A)$$

$$\frac{\tilde{\theta}_t - \tilde{\theta}_{t-1}}{\tilde{\eta}_t} = \frac{\gamma(\tilde{\theta}_{t-1} - \tilde{\theta}_{t-2})}{\tilde{\eta}_{t-1}} - \nabla_\theta \left(L(\tilde{\theta}_{t-1}) + \frac{\tilde{\lambda}_t}{2} \|\tilde{\theta}_{t-1}\|_2^2 \right). \quad (B)$$

If $\alpha \in \mathcal{I}$, then the schedules

$$\tilde{\eta}_t = \eta_0 \alpha^{-2t-1}, \quad (8)$$

$$\tilde{\lambda}_t = \Xi(\alpha) \alpha^{2t-1} + \frac{\gamma(1-\alpha)}{\eta_0 \alpha} \mathbb{1}\{t=0\} \quad (9)$$

ensure $\tilde{\theta}_t = \alpha^{-t}\theta_t$ for all $t \geq 0$; hence (A) and (B) generate identical functions.

Remark 6.3 (Parameter range and nonnegativity). Assume

$$\lambda\eta_0 \leq (1 - \sqrt{\gamma})^2, \quad (10)$$

$$\alpha_L < \alpha_- \quad (\text{equivalently, } \Delta_\lambda \geq 0). \quad (11)$$

Then the interval \mathcal{I} above is nonempty and the square-root term is real; both conditions hold for common hyperparameters in practice.

Consequences. The proof of Theorem 6.2 is in Appendix C. In the scale-invariant setting, this equivalence lets us pump parameter norms without changing $f(\theta)$, a lever we use to stress-test generalization measures. Applying this dial, we find that even the measure that looked most stable in our earlier probes—the standard parameter-space PAC-Bayes proxy PACBAYES_orig—fails catastrophically here: as the Exp++ factor grows, the proxy inflates by orders of magnitude while test error is essentially unchanged; see Appendix H.

7. Quantitative fragility: a scale-free instability score

The heuristic stress tests in Sections 3–5 show that several popular post-mortem measures are fragile. Here we provide

a complementary *quantitative lens*: scale-free statistics that capture how much a measure fluctuates among runs with (nearly) the same test error. These quantitative metrics of fragility can facilitate larger-scale comparisons between measures.

Setup. Fix a dataset/architecture group g with trained runs \mathcal{S}_g . For run $r \in \mathcal{S}_g$, let $\hat{\varepsilon}_r \in [0, 1]$ denote test error and $C_r \in (0, \infty)$ the value of a post-mortem measure C (e.g., a norm proxy). For an absolute error tolerance $\delta > 0$, define the close-error set

$$\Pi_\delta(\mathcal{S}_g) = \{(r, s) \in \mathcal{S}_g^2 : r < s, |\hat{\varepsilon}_r - \hat{\varepsilon}_s| \leq \delta\}. \quad (12)$$

Definition 7.1 (Conditional Measure Spread (CMS)). The CMS of C in group g at tolerance δ is

$$\text{CMS}_\delta(C; g) = \text{median}_{(r,s) \in \Pi_\delta(\mathcal{S}_g)} |\log C_r - \log C_s|. \quad (13)$$

Interpretation. e^{CMS_δ} is the typical multiplicative factor by which C varies across runs that are indistinguishable in test error up to δ (e.g., $\text{CMS}_\delta \approx \ln 2$ means a factor-two swing).

Randomness adjustment. To separate hyperparameter induced jumpiness from random-seed jitter, let H_r collect the training hyperparameters for run r (e.g., optimizer, learning rate, schedule flags, early-stopping rule, training-set size), and let seed_r be its random seed. Split close-error pairs into

$$\Pi_\delta^{\text{seed}}(g) = \{(r, s) \in \Pi_\delta(\mathcal{S}_g) : H_r = H_s, \text{seed}_r \neq \text{seed}_s\}, \quad (14)$$

$$\Pi_\delta^{\text{inter}}(g) = \{(r, s) \in \Pi_\delta(\mathcal{S}_g) : H_r \neq H_s\}. \quad (15)$$

Define the corresponding spreads

$$\text{CMS}_\delta^{\text{seed}}(C; g) = \text{median}_{(r,s) \in \Pi_\delta^{\text{seed}}(g)} |\log C_r - \log C_s|, \quad (16)$$

$$\text{CMS}_\delta^{\text{inter}}(C; g) = \text{median}_{(r,s) \in \Pi_\delta^{\text{inter}}(g)} |\log C_r - \log C_s|. \quad (17)$$

Definition 7.2 (eCMS (Excess CMS)). The seed-adjusted excess at matched error is

$$\text{eCMS}_\delta(C; g) = \left[\text{CMS}_\delta^{\text{inter}}(C; g) - \text{CMS}_\delta^{\text{seed}}(C; g) \right]_+. \quad (18)$$

Aggregation across groups. Let \mathcal{G} be the set of dataset/architecture groups. We summarize by medians across groups (and report coverage):

$$\text{CMS}_\delta^{\text{med}}(C) = \text{median}_{g \in \mathcal{G}} \{\text{CMS}_\delta(C; g)\}, \quad (19)$$

$$\text{eCMS}_\delta^{\text{med}}(C) = \text{median}_{g \in \mathcal{G}} \{\text{eCMS}_\delta(C; g)\}. \quad (20)$$

This “median-of-medians” is robust to heterogeneous group sizes and outliers.

How to read the scores.

- **CMS.** Values near 0 indicate a stable measure among equal-error runs; larger values mean greater local instability. (For reference, $\ln 2 \approx 0.69$, $\ln 3 \approx 1.10$ in the same log units.)
- **eCMS.** Values near 0 indicate that most equal-error variability is seed-level; large eCMS points to *hyperparameter-sensitive* jumpiness beyond seeds.
- **Effect of δ .** Decreasing δ tightens the notion of “equal-error.” Scores that remain large as $\delta \downarrow 0$ reflect genuinely volatile measures.

Properties and protocol. Both statistics are robust (medians) and *scale-free* (invariant under $C \mapsto aC$, $a > 0$). Unless noted otherwise we use absolute tolerances $\delta \in \{0.01, 0.02, 0.05\}$ (i.e., 1% - 5% of error), uniformly subsample pairs if they exceed a fixed budget, and report, for each measure, the medians $\text{CMS}_{\delta}^{\text{med}}$ and $\text{eCMS}_{\delta}^{\text{med}}$, along with the number of eligible pairs in (12)–(15) and the fraction of groups covered. Together, CMS and eCMS capture (i) local instability at matched error and (ii) the seed-adjusted component attributable to hyperparameters. Full experimental details, formal algorithms and tabulated results can be found in Appendix E.

8. Conclusion and discussion

We take a pragmatic view of generalization bounds: in modern deep learning they function best as measures to be judged by how they behave across data and training regimes rather than by worst-case tightness. Read this way, fragility becomes a key property to audit. With the task fixed and accuracy essentially steady, small and reasonable pipeline tweaks—changing the learning rate by a factor of ten, swapping ADAM for momentum SGD, toggling early stopping—can bend surrogate curves, invert trends, or inflate their scale. When the task complexity changes, via label corruption or by moving from MNIST to Fashion-MNIST to CIFAR-10, several surrogates fail to preserve the expected ordering or slope. Our scale-invariance construction makes this failure mode explicit: one can inflate parameter magnitudes without changing the predictor, and magnitude-sensitive post-mortems then balloon while test error does not. This gap underscores that properties of a single parameter vector need not reflect properties of the learned function.

The comparison between post-mortem diagnostics and the marginal-likelihood PAC–Bayes route in function space sharpens the lesson. This predictor can capture key trends with data complexity, including the slopes of learning curves. Given that the interaction between data and architecture is one of the key components of DNN performance that needs

explaining, the success of this bound, and its simple interpretation in terms of inductive bias at initialisation, provides a concrete foil against which parameter-space surrogates can be refined.

Looking forward, several concrete directions could strengthen this position:

- Design reparameterization-invariant, data-aware post-training diagnostics that borrow the Occam flavour of marginal likelihood while remaining practical at scale;
- build a public fragility benchmark and automated audit harness covering optimizer/schedule swaps, scale-symmetry probes, and data-complexity sweeps.
- Develop approximate function-space surrogates (finite-width corrections, amortized evidence estimators, ensembles as posteriors over functions) to make invariance-friendly predictors usable in routine training.
- Tie diagnostics to training dynamics by discouraging scale-only drift after interpolation or by incorporating function-space objectives during training.
- Extend evaluation beyond vision classification to sequence models, generative modelling, reinforcement learning, and explicit distribution shift, testing whether the same invariance principles hold.

9. Alternative Views

Reasonable researchers can disagree with our emphasis on parameter-space fragility. We highlight several viable counterpositions and address them in turn:

- **Optimizer sensitivity is signal, not noise.** Because implicit bias *drives* which predictor is learned, a useful measure should move with the training pipeline, not be invariant to it.
- **Post-mortem measures can be stabilized.** With the right reparameterization-aware definitions (e.g., normalized sharpness, margin distributions, distance from initialization), much of the apparent fragility disappears.
- **Function-space GP baselines are mis-specified for modern, finite-width practice.** GP priors, absence of data augmentation in the prior, and finite-width effects limit how decisively marginal-likelihood predictors should be used as a reference.

Optimizer sensitivity as a feature. It is widely thought that optimizer, schedule, and batch size are first-order determinants of generalization that *should* be reflected in generalization measures. This view points to well-documented

implicit-bias phenomena—e.g., margin growth under separable losses and optimizer-dependent convergence paths—that influence which classifier is ultimately selected (Soudry et al., 2018; Smith et al., 2017; Simsekli et al., 2019). From this perspective, the very invariances we prize risk washing out real, practically actionable differences between training recipes.

Response. We agree that optimizer choice can change the learned function and that a diagnostic should detect *functionally meaningful* changes. Our claim is narrower: diagnostics that swing under *pure scale drift* or minor hyperparameter nudges while test error and predictions remain essentially fixed can mislead day-to-day comparisons. This is why our audit always pairs any optimizer comparison with either (i) matched-prediction checkpoints (e.g., at the first 100%-accuracy crossing) or (ii) a symmetry lever that alters parameter scale without changing the predictor (§6). When pipeline changes *do* alter the predictor, a stable measure should move in tandem with test error; when they do not, a robust measure should be indifferent.

Stabilizing post-mortem diagnostics. A second objection holds that many post-training measures already address scale and parameterization issues. Normalized or reparameterization-aware sharpness correlates more reliably with generalization than raw curvature (Dinh et al., 2017; Tsuzuku et al., 2020; Kim et al., 2022; Jang et al., 2022); modeling the *distribution* of margins rather than the minimum improves predictiveness across runs (Jiang et al., 2018); reference-aware surrogates such as distance from initialization or movement from pretraining reduce width and scale artifacts and come with supporting analyses (Li et al., 2018; Neyshabur et al., 2017a; Zhou et al., 2021). On this view, fragility largely reflects naive implementations, not intrinsic flaws.

Response. We see these developments as complementary and encouraging. Our results target precisely such “best-effort” variants (normalized, margin-aware, reference-aware) and still uncover qualitative flips under mild pipeline changes when predictions are stable. We do not argue that post-mortems are without merit; rather, we argue they remain *fragile enough* that authors should routinely report their stability under the kinds of stressors we outline (§3–5), and prefer versions that (i) are explicitly invariant to layerwise rescalings, (ii) condition on matched prediction milestones, and (iii) are benchmarked against data-difficulty shifts and temporal drift after interpolation. In short, our audit is a bar to clear, not a dismissal of the enterprise.

Limits of function–space GP references. A third objection is that using a marginal-likelihood PAC–Bayes predictor as a baseline (Appendix F) overstates its practical authority. Since a GP is used to approximate the key marginal-

likelihood term in the bound, the ML-PACBayes predictor could be seen as a measure of the performance of the underlying GP for any given architecture–data combination. While GPs are known to closely match DNN performance on the datasets we test in this paper (Lee et al., 2020b), it is hard to see how one could untangle the effects of hyperparameters or optimiser choice in this approach, in other words, the kinds of questions that post-mortem bounds are trying to address. More generally, modern deep-learning models are finite-width, heavily augmented, and often trained far from the GP regime; priors that ignore augmentation, architectural quirks, or fine-tuned tokenization may be badly mis-specified. In addition, the bound controls the error of a stochastic Gibbs classifier drawn from a posterior over functions, not necessarily the deterministic network one actually deploys. Therefore, the GP route’s stability could stem from *omitting* factors that matter in practice (Lee et al., 2020b; Valle-Pérez & Louis, 2020).

Response. We agree that one of the most important questions that needs explaining in DNNs is how, when, and why finite-width networks outperform their infinite-width GP limits, in particular for settings where feature-learning is important (see e.g. (Goring et al., 2025) and references therein). We use the GP based marginal-likelihood bound as a *calibration* tool, not an oracle: it naturally encodes desirable invariances (insensitivity to parameter scale and optimizer path once the dataset is fixed) and for the cases we study, consistently tracks data difficulty and learning-curve scaling across families. Those properties make it a valuable foil for stress-testing post-mortem bounds. Where the GP prior is clearly misspecified (e.g., heavy augmentation or domains where feature-leaning is key), our recommendation is empirical: rerun the same fragility audit. If the GP predictor ceases to track error while a reparameterization-invariant post-mortem does, that is evidence *for* the importance of a post-mortem analysis in that regime.

Synthesis. These counterarguments motivate a middle path. Rather than elevating any single diagnostic, we advocate (i) reporting multiple invariance-aware post-mortem measures, (ii) auditing them with our stressors (learning-curve shape, temporal drift after interpolation, and data-complexity response), and (iii) anchoring interpretation with at least one function–space reference when feasible. This recognizes optimizer-dependent mechanisms while discouraging conclusions drawn from features (e.g., raw scale) that can be changed without affecting predictions.

Impact Statement

This is a position paper about evaluation practice. The main impact is methodological: a simple audit protocol and reporting guidelines that encourage robustness checks for

generalization measures. Potential positive impacts include more reliable model selection and clearer communication of limitations; potential negative impacts are minimal, as we do not propose deployable systems or datasets.

References

Andriushchenko, M. and Flammarion, N. Towards understanding sharpness-aware minimization. In *International Conference on Machine Learning*, pp. 639–668, 2022. URL <https://proceedings.mlr.press/v162/andriushchenko22a/andriushchenko22a.pdf>.

Anthony, M. and Bartlett, P. L. *Neural Network Learning - Theoretical Foundations*. 2002. URL http://www.cambridge.org/gb/knowledge/isbn/item1154061/?site_locale=en_GB.

Arora, S., Ge, R., Neyshabur, B., and Zhang, Y. Stronger generalization bounds for deep nets via a compression approach. In *Proceedings of the 35th International Conference on Machine Learning*, Proceedings of Machine Learning Research, 10–15 Jul 2018a. doi: 10.48550/arxiv.1802.05296. URL <https://doi.org/10.48550/arxiv.1802.05296>.

Arora, S., Li, Z., and Lyu, K. Theoretical analysis of auto rate-tuning by batch normalization. *arXiv preprint arXiv:1812.03981*, 2018b. URL <https://arxiv.org/abs/1812.03981>.

Arora, S., Du, S. S., Hu, W., Li, Z., and Wang, R. Fine-grained analysis of optimization and generalization for overparameterized two-layer neural networks. *arXiv preprint arXiv:1901.08584*, 2019. URL <https://arxiv.org/abs/1901.08584>.

Bahri, Y., Dyer, E., Kaplan, J., Lee, J., and Sharma, U. Explaining scaling laws of neural network generalization. 2021.

Bartlett, P. L. and Mendelson, S. Rademacher and gaussian complexities: Risk bounds and structural results. *Journal of Machine Learning Research*, 2001. doi: 10.1007/3-540-44581-1_15. URL https://doi.org/10.1007/3-540-44581-1_15.

Bartlett, P. L., Foster, D. J., and Telgarsky, M. Spectrally-normalized margin bounds for neural networks. In *Advances in Neural Information Processing Systems (NeurIPS)*, 2017. doi: 10.48550/arxiv.1706.08498. URL <https://doi.org/10.48550/arxiv.1706.08498>.

Bartlett, P. L., Long, P. M., Lugosi, G., and Tsigler, A. Benign overfitting in linear regression. *Proceedings of the National Academy of Sciences*, 117(48):30063–30070, 2020. doi: 10.1073/pnas.1907378117. URL <https://doi.org/10.1073/pnas.1907378117>.

Belkin, M., Hsu, D., Ma, S., and Mandal, S. Reconciling modern machine-learning practice and the classical bias–variance trade-off. *Proceedings of the National Academy of Sciences*, 116(32):15849–15854, 2019. doi: 10.1073/pnas.1903070116. URL <https://doi.org/10.1073/pnas.1903070116>.

Blier, L. and Ollivier, Y. The description length of deep learning models. *arXiv preprint arXiv:1802.07044v5*, 2018. URL <https://arxiv.org/abs/1802.07044v5>.

Bousquet, O. and Elisseeff, A. Stability and generalization. *J. Mach. Learn. Res.*, 2:499–526, 2002. URL <https://jmlr.org/papers/v2/bousquet02a.html>.

Catoni, O. *PAC-Bayes Bounds for Supervised Classification*. 2007. URL https://doi.org/10.1007/978-3-319-21852-6_20.

Cohen, J., Duchi, J., Hasani, R., et al. The edge of stability: Test loss can be lower than training loss and nonconvexity. In *International Conference on Learning Representations (ICLR)*, 2021. URL <https://arxiv.org/abs/2103.06886>.

Dinh, L., Pascanu, R., Bengio, S., and Bengio, Y. Sharp minima can generalize for deep nets. *arXiv preprint arXiv:1703.04933*, 2017. URL <https://arxiv.org/abs/1703.04933>.

Dziugaite, Gintare Karolina and, D. M. R. Data-dependent pac-bayes priors via differential privacy. In *NeurIPS*, 2018. URL <https://proceedings.neurips.cc/paper/2018/hash/9a0ee0a9e7a42d2d69b8f86b3a0756b1-Abstract.html>.

Dziugaite, G. K. and Roy, D. M. Computing nonvacuous generalization bounds for deep (stochastic) neural networks via pac-bayes. In *International Conference on Learning Representations (ICLR)*, 2017. URL <https://openreview.net/forum?id=SkvQ7zPE->.

Dziugaite, G. K., Drouin, A., Neal, B., Rajkumar, N., Caballero, E., Wang, L., Mitliagkas, I., and Roy, D. M. In search of robust measures of generalization. In *Advances in Neural Information Processing Systems (NeurIPS)*, 2020a. doi: 10.48550/arxiv.2010.11924. URL <https://doi.org/10.48550/arxiv.2010.11924>.

Dziugaite, G. K., Drouin, A., Neal, B., Rajkumar, N., Caballero, E., Wang, L., Mitliagkas, I., and Roy, D. M. In search of robust measures of generalization. *arXiv*

preprint arXiv:2010.11924, 2020b. URL <https://arxiv.org/abs/2010.11924>.

Foret, P., Kleiner, A., Mobahi, H., and Neyshabur, B. Sharpness-aware minimization for efficiently improving generalization. *arXiv preprint arXiv:2010.01412*, 2020. URL <https://arxiv.org/abs/2010.01412>.

Gastpar, M., Nachum, I., Shafer, J., and Weinberger, T. Fantastic generalization measures are nowhere to be found. In *International Conference on Learning Representations (ICLR)*, 2023. doi: 10.48550/arxiv.2309.13658. URL <https://doi.org/10.48550/arxiv.2309.13658>.

Golowich, N., Rakhlin, A., and Shamir, O. Size-independent sample complexity of neural networks. In *Conference On Learning Theory*, pp. 297–299, 2018. URL <http://proceedings.mlr.press/v75/golowich18a/golowich18a.pdf>.

Gonon, A., Brisebarre, N., Riccietti, E., and Gribonval, R. A path-norm toolkit for modern networks: consequences, promises and challenges. *arXiv preprint arXiv:2310.01225*, 2023. URL <https://arxiv.org/abs/2310.01225>. ICLR 2024 Spotlight.

Goring, N. A., London, C., Erturk, A. H., Mingard, C., Nam, Y., and Louis, A. A. Feature learning is decoupled from generalization in high capacity neural networks. *arXiv preprint arXiv:2507.19680*, 2025.

Gouk, H., Frank, E., Pfahringer, B., and Cree, M. J. Regularisation of neural networks by enforcing lipschitz continuity. In *International Conference on Learning Representations (ICLR)*, 2020. doi: 10.1007/s10994-020-05929-w. URL <https://doi.org/10.1007/s10994-020-05929-w>.

Hardt, M., Recht, B., and Singer, Y. Train faster, generalize better: Stability of stochastic gradient descent. *arXiv preprint arXiv:1509.01240v2*, 2015. URL <https://arxiv.org/abs/1509.01240v2>.

Hestness, J., Narang, S., Ardalani, N., Diamos, G., Jun, H., Kianinejad, H., Patwary, M. M. A., Yang, Y., and Zhou, Y. Deep learning scaling is predictable, empirically. In *International Conference on Learning Representations (ICLR) Workshop*, 2017. doi: 10.48550/arxiv.1712.00409. URL <https://doi.org/10.48550/arxiv.1712.00409>.

Hochreiter, S. and Schmidhuber, J. Flat minima. *Neural Computation*, 9(1):1–42, 1997. doi: 10.1162/neco.1997.9.1.1. URL <https://doi.org/10.1162/neco.1997.9.1.1>.

Hoffer, E., Hubara, I., and Soudry, D. Train longer, generalize better: closing the generalization gap in large batch training of neural networks. In *Advances in neural information processing systems*, 2017. doi: 10.48550/arxiv.1705.08741. URL <https://doi.org/10.48550/arxiv.1705.08741>.

Hoffmann, J., Borgeaud, S., Mensch, A., Buchatskaya, E., Cai, T., Rutherford, E., Casas, D. d. L., Hendricks, L. A., Welbl, J., Clark, A., Hennigan, T., Noland, E., Milligan, K., Driessche, G. v. d., Damoc, B., Guy, A., Osindero, S., Simonyan, K., Elsen, E., Rae, J. W., Vinyals, O., and Sifre, L. Training compute-optimal large language models. In *arXiv preprint arXiv:2203.15556*, 2022. doi: 10.48550/arxiv.2203.15556. URL <https://doi.org/10.48550/arxiv.2203.15556>.

Izmailov, P., Podoprikin, D., Garipov, T., Vetrov, D., and Wilson, A. G. Averaging weights leads to wider optima and better generalization. *arXiv preprint arXiv:1803.05407*, 2018. URL <https://arxiv.org/abs/1803.05407>.

Jacot, A. P., Gabriel, F., and Hongler, C. Neural tangent kernel: Convergence and generalization in neural networks. In *Advances in neural information processing systems*, 2018. doi: 10.48550/arxiv.1806.07572. URL <https://doi.org/10.48550/arxiv.1806.07572>.

Jang, C., Lee, S., Park, F., and Noh, Y.-K. A reparametrization-invariant sharpness measure based on information geometry. *Advances in neural information processing systems*, 35:27893–27905, 2022.

Jastrzebski, S., Kenton, Z., Arpit, D., Ballas, N., Fischer, A., Bengio, Y., and Storkey, A. Three factors influencing minima in sgd. In *International Conference on Artificial Intelligence and Statistics (AISTATS) Workshop*, 2017. doi: 10.48550/arxiv.1711.04623. URL <https://doi.org/10.48550/arxiv.1711.04623>.

Jiang, Y., Krishnan, D., Mobahi, H., and Bengio, S. Predicting the generalization gap in deep networks with margin distributions. *arXiv preprint arXiv:1810.00113*, 2018. URL <https://arxiv.org/abs/1810.00113>.

Jiang, Y., Neyshabur, B., Mobahi, H., Krishnan, D., and Bengio, S. Fantastic generalization measures and where to find them. In *International Conference on Learning Representations (ICLR)*, 2019a. doi: 10.48550/arxiv.1912.02178. URL <https://doi.org/10.48550/arxiv.1912.02178>.

Jiang, Y., Neyshabur, B., Mobahi, H., Krishnan, D., and Bengio, S. Fantastic generalization measures and where to find them. *arXiv preprint arXiv:1912.02178*, 2019b. URL <https://arxiv.org/abs/1912.02178>.

Kaplan, J., McCandlish, S., Henighan, T., Brown, T. B., Chess, B., Child, R., Gray, S., Radford, A., Wu, J., and Amodei, D. Scaling laws for neural language models. In *arXiv preprint arXiv:2001.08361*, 2020. doi: 10.48550/arxiv.2001.08361. URL <https://doi.org/10.48550/arxiv.2001.08361>.

Keskar, N. S., Mudigere, D., Nocedal, J., Smelyanskiy, M., and Tang, P. T. P. On large-batch training for deep learning: Generalization gap and sharp minima. In *ICLR*, 2017. URL <https://openreview.net/forum?id=H1oyR1Ygg>.

Kim, S., Park, S., Kim, K., and Yang, E. Scale-invariant bayesian neural networks with connectivity tangent kernel. *arXiv preprint arXiv:2209.15208*, 2022.

Koltchinskii, V. Rademacher penalties and structural risk minimization. *IEEE Transactions on Information Theory*, 47(5):1902–1914, 2001. doi: 10.1109/18.930926. URL <https://doi.org/10.1109/18.930926>.

Kwon, J., Kim, J.-S., Park, H., and Choi, I. K. Asam: Adaptive sharpness-aware minimization for scale-invariant learning of deep neural networks. In *International Conference on Machine Learning (ICML)*, 2021. doi: 10.48550/arxiv.2102.11600. URL <https://doi.org/10.48550/arxiv.2102.11600>.

Langford, J. and Shawe-Taylor, J. Pac-bayes & margins. In *NIPS*, 2002. URL <https://proceedings.neurips.cc/paper/2002/hash/68d309812548887400e375eaa036d2f1-Abstract.html>.

Lee, J., Schoenholz, S. S., Pennington, J., Adlam, B., Xiao, L., Novak, R., and Sohl-Dickstein, J. Finite versus infinite neural networks: an empirical study. *arXiv preprint arXiv:2007.15801v2*, 2020a. URL <https://arxiv.org/abs/2007.15801v2>.

Lee, J., Xiao, L., Schoenholz, S. S., Bahri, Y., Novak, R., Sohl-Dickstein, J., and Pennington, J. Wide neural networks of any depth evolve as linear models under gradient descent $\|\sup_{\zeta} \cdot\|_{\sup_{\zeta}}$. In *Advances in Neural Information Processing Systems (NeurIPS)*, 2020b. doi: 10.1088/1742-5468/abc62b. URL <https://doi.org/10.1088/1742-5468/abc62b>.

Li, H., Xu, Z., Taylor, G., Studer, C., and Goldstein, T. Visualizing the loss landscape of neural nets. In *Advances in Neural Information Processing Systems (NeurIPS)*, 2017. doi: 10.48550/arxiv.1712.09913. URL <https://doi.org/10.48550/arxiv.1712.09913>.

Li, X., Lu, J., Wang, Z., Haupt, J., and Zhao, T. On tighter generalization bound for deep neural networks: Cnns, resnets, and beyond. *arXiv preprint arXiv:1806.05159*, 2018. URL <https://arxiv.org/abs/1806.05159>.

Li, Z. and Arora, S. An exponential learning rate schedule for deep learning. *arXiv preprint arXiv:1910.07454*, 2019. URL <https://arxiv.org/abs/1910.07454>.

Lin, M., Chen, Q., and Yan, S. Network in network. *arXiv preprint arXiv:1312.4400*, 2013.

Lotfi, S., Finzi, M., Kapoor, S., Potapczynski, A., Goldblum, M., and Wilson, A. G. Pac-bayes compression bounds so tight that they can explain generalization. *Advances in Neural Information Processing Systems*, 35:31459–31473, 2022. URL <https://doi.org/10.48550/arxiv.2211.13609>.

McAllester, D. A. Some pac-bayesian theorems. *Machine Learning*, 37(3):355–363, 1999. doi: 10.1023/a:1007618624809. URL <https://doi.org/10.1023/a:1007618624809>.

McCandlish, S., Kaplan, J., Amodei, D., and Team, O. D. An empirical model of large-batch training. *arXiv preprint arXiv:1812.06162*, 2018. URL <https://arxiv.org/abs/1812.06162>.

Mendelson, S. A few notes on statistical learning theory. In *Machine Learning Summer School*. Wiley, 2002. doi: 10.1007/3-540-36434-X_1. URL https://doi.org/10.1007/3-540-36434-X_1.

Nagarajan, V. and Kolter, J. Z. Uniform convergence may be unable to explain generalization in deep learning. *arXiv preprint arXiv:1902.04742v4*, 2019. URL <https://arxiv.org/abs/1902.04742v4>.

Nam, Y., Mingard, C., Lee, S. H., Hayou, S., and Louis, A. Visualising feature learning in deep neural networks by diagonalizing the forward feature map. *arXiv e-prints*, pp. arXiv–2410, 2024.

Neyshabur, B., Tomioka, R., and Srebro, N. Norm-based capacity control in neural networks. In *Conference on Learning Theory*, pp. 1376–1401, 2015. URL <http://proceedings.mlr.press/v40/Neyshabur15.pdf>.

Neyshabur, B., Bhojanapalli, S., McAllester, D., and Srebro, N. Exploring generalization in deep learning. *arXiv preprint arXiv:1706.08947v2*, 2017a. URL <https://arxiv.org/abs/1706.08947v2>.

Neyshabur, B., Bhojanapalli, S., and Srebro, N. A pac-bayesian approach to spectrally-normalized margin bounds for neural networks. *arXiv preprint arXiv:1707.09564*, 2017b. URL <https://arxiv.org/abs/1707.09564>.

Neyshabur, B., Li, Z., Bhojanapalli, S., LeCun, Y., and Srebro, N. The role of over-parametrization in generalization of neural networks. In *International Conference on Learning Representations*, 2019. URL <https://openreview.net/forum?id=BygfhAcYX>.

Novak, R., Bahri, Y., Abolafia, D. A., Pennington, J., and Sohl-Dickstein, J. Sensitivity and generalization in neural networks: an empirical study. In *International Conference on Learning Representations (ICLR)*, 2018. doi: 10.48550/arxiv.1802.08760. URL <https://doi.org/10.48550/arxiv.1802.08760>.

Paszke, A., Gross, S., Chintala, S., Chanan, G., Yang, E. Z., DeVito, Z., Lin, Z., Desmaison, A., Antiga, L., and Lerer, A. Automatic differentiation in pytorch. 2017. URL <https://openreview.net/pdf?id=BJJsrnfCZ>.

Pérez-Ortiz, M., Rivasplata, O., Shawe-Taylor, J., and Szepesvári, C. Tighter risk certificates for neural networks. *The Journal of Machine Learning Research*, 2020. doi: 10.48550/arxiv.2007.12911. URL <https://doi.org/10.48550/arxiv.2007.12911>.

Rodríguez-Gálvez, B., Thobaben, R., and Skoglund, M. More pac-bayes bounds: From bounded losses, to losses with general tail behaviors, to anytime validity. *Journal of Machine Learning Research*, 25(110):1–43, 2024. URL <http://jmlr.org/papers/v25/23-1360.html>.

Russo, D. and Zou, J. Controlling bias in adaptive data analysis using information theory. In Gretton, A. and Robert, C. C. (eds.), *Proceedings of the 19th International Conference on Artificial Intelligence and Statistics*, volume 51 of *Proceedings of Machine Learning Research*, pp. 1232–1240, Cadiz, Spain, 09–11 May 2016. PMLR. URL <https://proceedings.mlr.press/v51/russo16.html>.

Seeger, M. Pac-bayesian generalization error bounds for gaussian process classification. In *Advances in Neural Information Processing Systems (NeurIPS)*, 2002.

Simsekli, U., Sagun, L., and Gurbuzbalaban, M. A tail-index analysis of stochastic gradient noise in deep neural networks. In *International Conference on Machine Learning*, pp. 5827–5837. PMLR, 2019. URL <https://proceedings.mlr.press/v97/simsekli19a.html>.

Smith, S. L., Kindermans, P.-J., Ying, C., and Le, Q. V. Don’t decay the learning rate, increase the batch size. *arXiv preprint arXiv:1711.00489*, 2017. URL <https://arxiv.org/abs/1711.00489>.

Soudry, D., Hoffer, E., Nacson, M. S., Gunasekar, S., and Srebro, N. The implicit bias of gradient descent on separable data. *Journal of Machine Learning Research*, 2018. doi: 10.5555/3291125.3309632. URL <https://doi.org/10.5555/3291125.3309632>.

Spigler, S., Geiger, M., and Wyart, M. Asymptotic learning curves of kernel methods: empirical data v.s. teacher-student paradigm. *arXiv preprint arXiv:1905.10843*, 2019. URL <https://arxiv.org/abs/1905.10843>.

Taiji Suzuki, Hiroshi Abe, T. N. Compression based bound for non-compressed network: unified generalization error analysis of large compressible deep neural network. volume 8, 2020. URL <https://arxiv.org/abs/1909.11274>.

Tsuzuku, Y., Sato, I., and Sugiyama, M. Normalized flat minima: Exploring scale invariant definition of flat minima for neural networks using pac-bayesian analysis. In *International Conference on Machine Learning*, pp. 9636–9647. PMLR, 2020. URL <https://arxiv.org/abs/1901.04653>.

Valle-Pérez, G. and Louis, A. A. Generalization bounds for deep learning. *arXiv preprint arXiv:2012.04115*, 2020. URL <https://arxiv.org/abs/2012.04115>.

Valle-Pérez, G., Camargo, C. Q., and Louis, A. A. Deep learning generalizes because the parameter-function map is biased towards simple functions. *arXiv preprint arXiv:1805.08522*, 2018. URL <https://arxiv.org/abs/1805.08522>.

Xu, A. and Raginsky, M. Information-theoretic analysis of generalization capability of learning algorithms. *Advances in Neural Information Processing Systems*, 30, 2017. URL <https://arxiv.org/abs/1705.07809>.

Yoshida, Y. and Miyato, T. Spectral norm regularization for improving the generalizability of deep learning. *arXiv preprint arXiv:1705.10941*, 2017. URL <https://arxiv.org/abs/1705.10941>.

Zhang, C., Bengio, S., Hardt, M., Recht, B., and Vinyals, O. Understanding deep learning requires rethinking generalization. *arXiv preprint arXiv:1611.03530*, 2016. URL <https://arxiv.org/abs/1611.03530>.

Zhang, S. and Louis, A. Closed-form ℓ_r norm scaling with data for overparameterized linear regression and diagonal linear networks under ℓ_p bias. *arXiv preprint arXiv:2509.21181*, 2025. URL <https://arxiv.org/abs/2509.21181>.

Zhang, S., Reid, I., Pérez, G. V., and Louis, A. Why flatness does and does not correlate with generalization for deep neural networks. *arXiv preprint arXiv:2103.06219*, 2021.
URL <https://arxiv.org/abs/2103.06219>.

Zhou, Y., Liang, Y., and Zhang, H. Understanding generalization error of sgd in nonconvex optimization. *stat*, 2021. doi: 10.1007/s10994-021-06056-w. URL <https://doi.org/10.1007/s10994-021-06056-w>.

A. Training-hyperparameter fragility for all measures

In this section we give concise definitions of the measures we study (aligning notation with prior large-scale evaluations) and provide additional experimental evidence beyond the main text (Dziugaite et al., 2020b; Jiang et al., 2019b). We then present figure-backed comparisons where small learning-rate or optimizer tweaks trigger qualitatively different curve shapes for the surrogate—plateaus, rebounds, late spikes, and crossings—while the accompanying accuracy curves remain comparatively calm.

A.1. Measures considered

We adopt the categories and normalizations used by prior experimental studies of generalization measures (Jiang et al., 2019b; Dziugaite et al., 2020b); for exact constants and implementation choices, see App. C.6 of Dziugaite et al. (2020b). Let a d -layer network have layer weights $\{W_i\}_{i=1}^d$ with initialization $\{W_i^0\}$; write $\|\cdot\|_F$ and $\|\cdot\|_2$ for Frobenius and spectral norms; let n denote training-set size and γ a robust (e.g., 10th-percentile) training margin.

- **Frobenius distances.** Layerwise distances from initialization and norm aggregates, e.g.

$$C_{\text{FrobDist}} = \sqrt{\sum_{i=1}^d \|W_i - W_i^0\|_F^2 / n}, \quad C_{\text{param}} = \sqrt{\sum_{i=1}^d \|W_i\|_F^2 / n}.$$

- **Inverse margin.** A margin-based surrogate,

$$C_{\text{inv-margin}} \propto \frac{\sqrt{n}}{\gamma}.$$

- **Spectral metrics.** Products/means and distances in spectral norm, e.g.

$$C_{\Pi \text{ spec}} = \sqrt{\prod_{i=1}^d \|W_i\|_2^2 / n}, \quad C_{\text{DistSpecInit}} = \sqrt{\sum_{i=1}^d \|W_i - W_i^0\|_2^2 / n}.$$

- **Combined spectral–Frobenius ratio.** We follow the combined ratio used in prior large-scale studies (App. C.6 of Dziugaite et al., 2020a), denoted `FRO_OVER_SPEC`, which normalizes Frobenius quantities by spectral ones to reduce raw scale effects. We report it alongside its constituents in our plots.

- **PAC-Bayes families and flatness proxies.** Bounds/proxies parameterized by posterior radii σ (and magnitude-aware σ_0), e.g.

$$C_{\text{PACBAYES-ORIG}} = \frac{1}{\sqrt{n}} \sqrt{\frac{\|w\|_2^2}{4\sigma^2} + \log\left(\frac{n}{\delta}\right) + 10}, \quad C_{\text{Flatness}} = \frac{1}{\sigma\sqrt{n}}, \quad C_{\text{MAG-Flatness}} = \frac{1}{\sigma_0\sqrt{n}}.$$

- **Path norms.** With $w = \text{vec}(W_1, \dots, W_d)$ and $f_{w^2}(\mathbf{1})[i]$ the i th logit when all weights are squared elementwise and the input is all ones,

$$C_{\text{path.norm}} = \sqrt{\sum_i f_{w^2}(\mathbf{1})[i] / n}, \quad C_{\text{path.norm-over-margin}} = \sqrt{\sum_i f_{w^2}(\mathbf{1})[i] / (\gamma^2 n)}.$$

- **VC-dimension proxy (parameter count).** A coarse parameter-count surrogate,

$$C_{\text{params}} = \sqrt{\sum_{i=1}^d k_i^2 c_{i-1} (c_i + 1) / n},$$

with kernel sizes k_i and channel counts c_i .

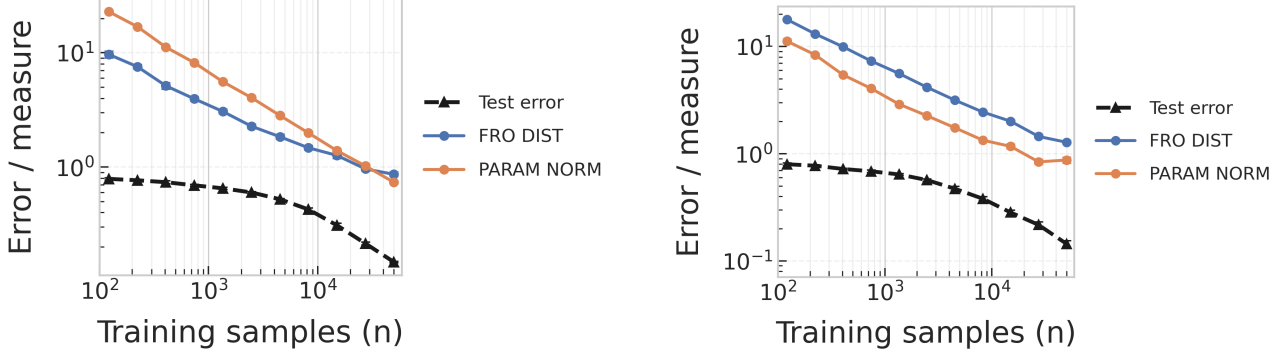


Figure S1. Frobenius distance, ResNet-50 on CIFAR-10 (Adam). Left: $\eta=10^{-3}$ shows a plateau and late collapse; right: $\eta=10^{-2}$ decays smoothly while accuracy tracks similarly.

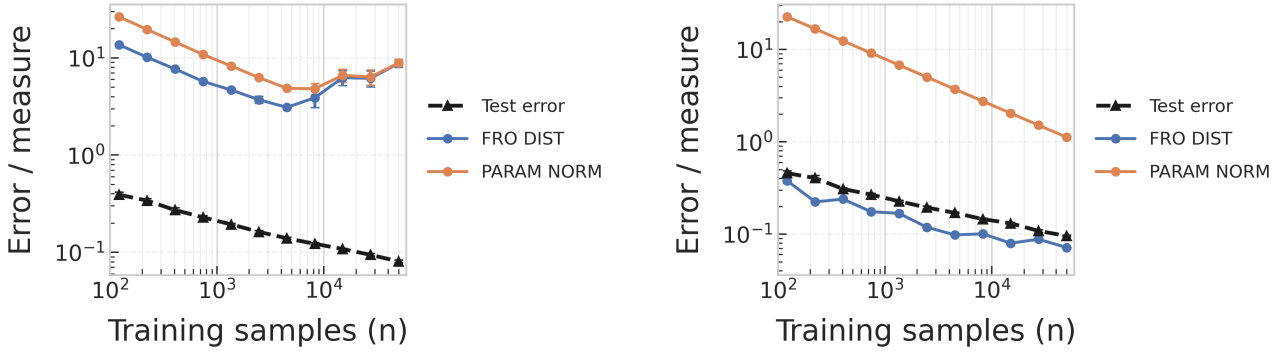


Figure S2. Frobenius distance, DenseNet-121 on FashionMNIST ($\eta=10^{-2}$). Left: ADAM yields a U-shape; right: SGD+mom declines nearly log-linearly; in both cases test accuracy evolves similarly.

A.2. Frobenius distance

Two qualitatively different shapes appear when only the learning rate or optimizer changes, and they are visible in Fig. S1 and Fig. S2. On RESNET-50/CIFAR-10 with Adam, $\eta=10^{-3}$ produces a broad plateau followed by a late collapse, whereas $\eta=10^{-2}$ decays smoothly throughout (compare left vs. right in Fig. S1). On DENSENET-121/FashionMNIST at fixed $\eta=10^{-2}$, Adam's curve is U-shaped (drop then rebound), while momentum SGD traces a near log-linear decline (left vs. right in Fig. S2); the accuracy curves remain closely aligned in both pairs.

A.3. Inverse margin

Figure S3 (left vs. right) shows that for RESNET-50/CIFAR-10 with Adam, $\eta=10^{-3}$ produces a smooth, power-law-like decline in inverse margin, whereas $\eta=10^{-2}$ stalls mid-training before resuming its drop; this kink has no analogue in the accuracy curve. At fixed $\eta=10^{-2}$ on FCN/FashionMNIST, ADAM develops a clear bump after roughly 10^3 samples while SGD's curve decreases monotonically (Fig. S4); again, both reach similar generalization.

A.4. Spectral metrics

Spectral surrogates display late spikes and order reversals under the same minimal tweaks. With DENSENET-121/FashionMNIST and Adam, $\eta=10^{-3}$ sends the distance-from-initialization in spectral norm down and then sharply up late in training, crossing the *FRO-OVER-SPEC* curve, whereas $\eta=10^{-2}$ keeps both traces monotone but flips their ordering (compare panels in Fig. S5). On RESNET-50/FashionMNIST at $\eta=10^{-2}$, ADAM shows a valley then rise, while SGD declines steadily (Fig. S6); accuracy curves overlap in both pairs.

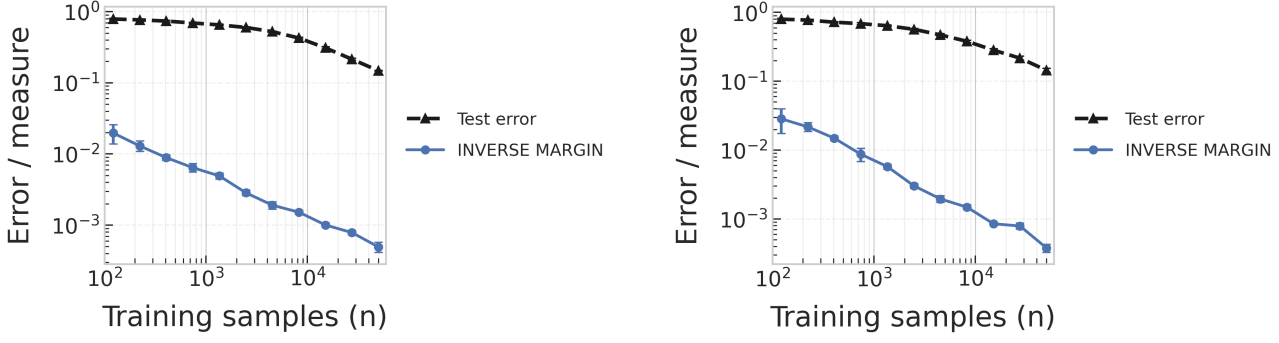


Figure S3. Inverse margin, ResNet-50 on CIFAR-10 (Adam). Left: $\eta=10^{-3}$ decays smoothly; right: $\eta=10^{-2}$ stalls then resumes, a kink absent from the accuracy curve.

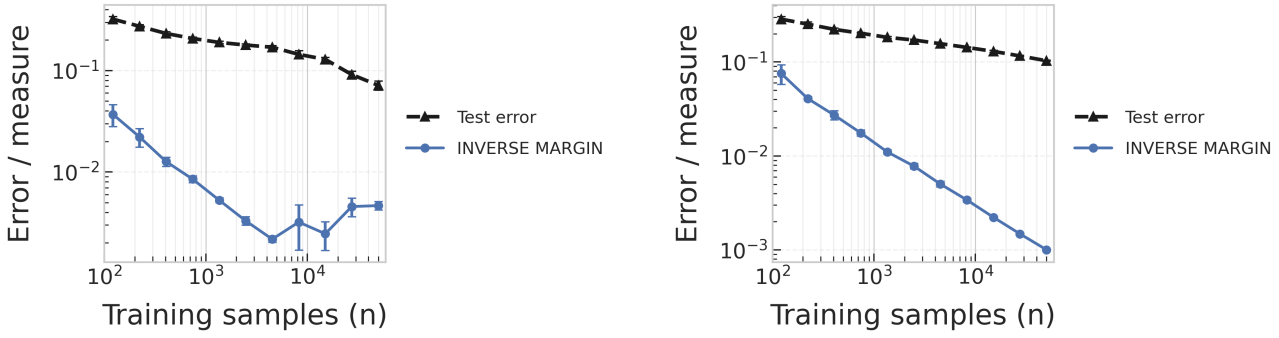


Figure S4. Inverse margin, FCN on FashionMNIST ($\eta=10^{-2}$). Left: ADAM develops a mid-course bump; right: SGD+mom is monotone; both generalize similarly.

A.5. PAC-Bayes bounds

Optimizer swaps and moderate learning-rate changes also produce curved versus straight “bound profiles” and late order crossings. For RESNET-50/FashionMNIST at $\eta=10^{-2}$, ADAM yields kinked “banana” trajectories across variants, whereas SGD renders near-straight lines (Fig. S7). Holding ADAM fixed and raising η from 10^{-3} to 10^{-2} reorders the variants late in training—for example, PACBAYES MAG and PACBAYES ORIG swap rank—even though accuracy shows no such crossing (Fig. S8).

A.6. VC-dimension proxy (robust baseline)

As a control, Fig. S9 shows that the parameter-count proxy for RESNET-50/CIFAR-10 with ADAM is strikingly shape-stable across $\eta=10^{-3}$ and $\eta=10^{-2}$: both traces are near-identical monotone decays, tracking one another while accuracy also aligns. This pair serves as a rare counterexample resistant to qualitative shifts.

Across all families above, the figures make a consistent point: changing only the learning rate or swapping the optimizer can reshape the surrogate’s learning curve—introducing plateaus, rebounds, late spikes, or crossings—with a commensurate shift in test accuracy. This shape-level fragility extends far beyond Path norms and cautions against reading causal explanations of generalization from any single surrogate without dedicated stress tests (Dziugaite et al., 2020b; Jiang et al., 2019b).

B. Additional temporal behavior results: optimizer sensitivity across measure families

This section extends the temporal analysis in Section 4 by holding the task and hyperparameters fixed and changing only the optimizer. We train ResNet-50 on FashionMNIST with learning rate 0.01 and no early stopping, and we track each measure across epochs. All panels use a logarithmic epoch axis; this makes the early regime and successive orders of magnitude more

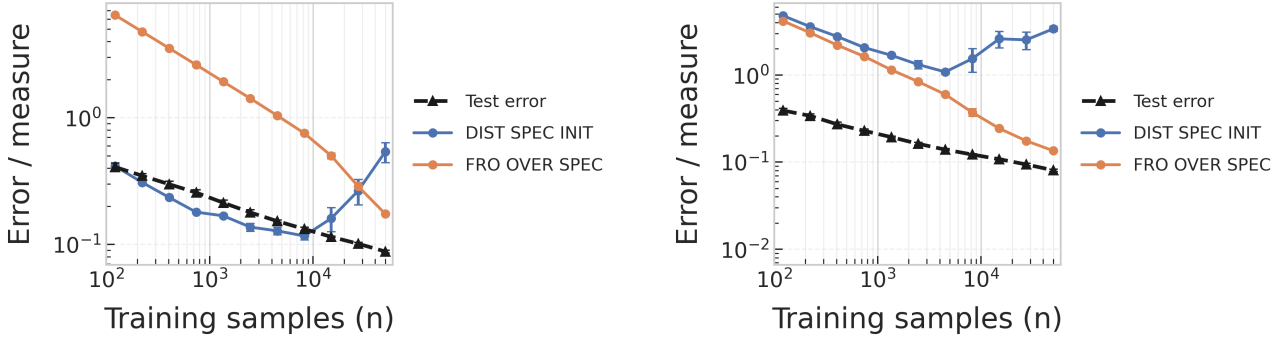


Figure S5. Spectral metrics, DenseNet-121 on FashionMNIST (Adam). Left: $\eta=10^{-3}$ drops then spikes, crossing FRO-OVER-SPEC; right: $\eta=10^{-2}$ stays monotone but reverses ordering.

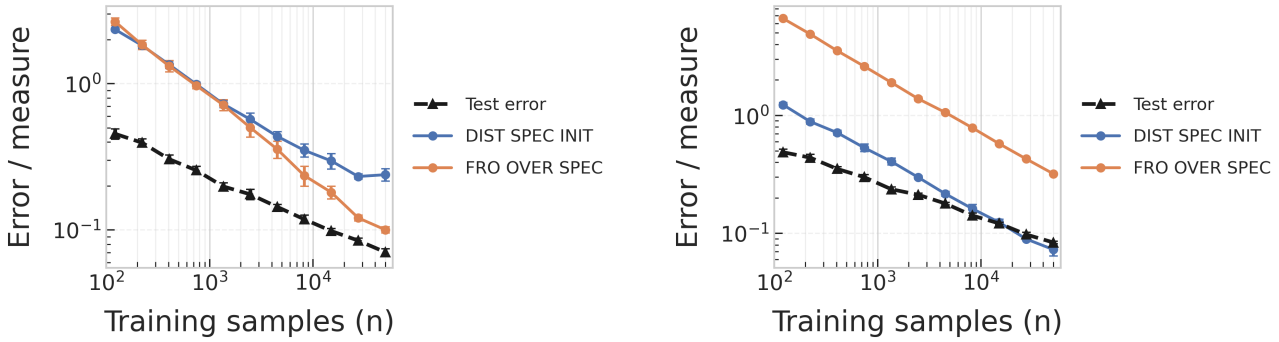


Figure S6. Spectral metrics, ResNet-50 on FashionMNIST ($\eta=10^{-2}$). Left: ADAM exhibits a valley then rise; right: SGD+mom declines steadily; accuracy is similar.

legible, while very late additive-only epochs occupy little horizontal extent unless they span a substantial multiplicative range. The red dashed vertical line in every panel marks the first epoch at which training accuracy reaches 100%; on a log axis this event is still easy to spot, but short post-interpolation intervals can appear visually narrow if they do not cover a large multiplicative window. To avoid duplication with the main text, we omit the path-norm panels here and focus on complementary families whose behavior further illustrates optimizer sensitivity.

The PAC-Bayes family provides a clean illustration of this theme. Under ADAM, multiple bounds show slow, persistent growth after interpolation; on a log-time axis this appears as a steady positive slope across late decades of epochs, most clearly for PACBAYES_ORIG and PACBAYES_INIT. With momentum SGD, the same curves remain essentially flat within error bars once the dashed line is crossed, and on the log axis they sit nearly horizontal, emphasizing stability rather than drift.

Measures tied to weight scale show the starker divergence. In the Frobenius panel, ADAM drives both the distance to initialization and the parameter norm upward almost monotonically after the model has interpolated; on a log-time axis this shows up as a persistent positive slope across late epochs. By contrast, momentum SGD leaves both traces effectively horizontal once the dashed line is passed, highlighting a stable plateau.

Not every family bends under this perturbation. Both optimizers rapidly reduce the inverse-margin surrogate early in training and then hold it near a floor. The log-time axis spreads out the initial drop, making the shared shape and timing transparent; ADAM settles at a slightly higher level, but the trajectories otherwise coincide.

Spectral surrogates reveal a subtler but consistent imprint. Under ADAM, the distance from initialization in spectral norm drifts upward over time; on log time the slope is small but positive beyond the dashed line. Under momentum SGD, the same quantity gently decreases from a plateau, appearing as a mild negative slope. The ratio FRO_OVER_SPEC also separates in level, hinting that the optimizer reshapes how mass is distributed across singular directions even when predictive performance is unchanged.

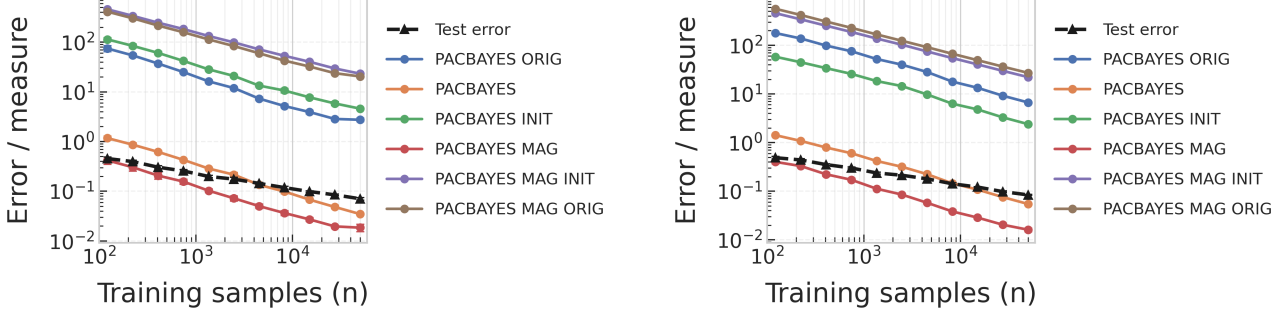


Figure S7. PAC-Bayes, ResNet-50 on FashionMNIST ($\eta=10^{-2}$). Left: ADAM produces curved, kinked trajectories; right: SGD+mom is nearly straight; test error changes little.

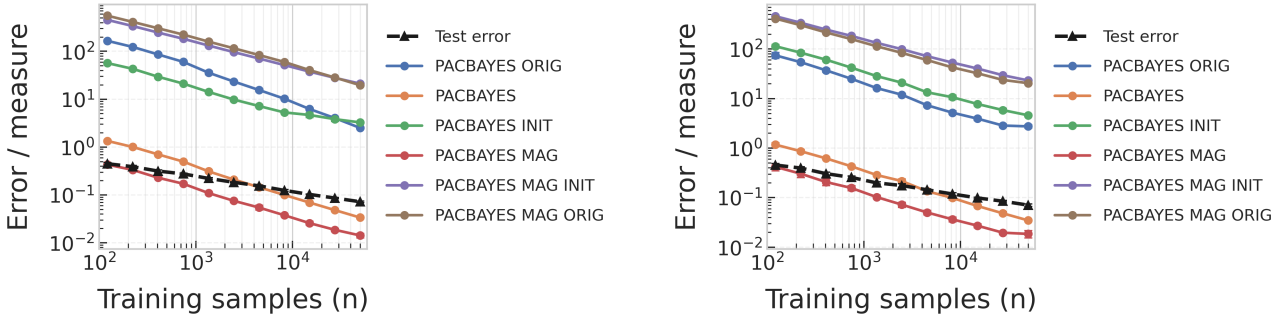


Figure S8. PAC-Bayes, ResNet-50 on FashionMNIST (Adam). Left: $\eta=10^{-3}$; right: $\eta=10^{-2}$. Increasing η induces late-training order swaps (e.g., MAG vs. ORIG) absent from the accuracy curves.

As a neutral reference, the VC-dimension proxy behaves identically across optimizers by construction, and the accompanying generalization error follows the same calm trajectory. The log-time axis makes this invariance explicit: the traces remain overlapped across decades of epochs, serving as anchors that remind us not all measures are sensitive to the optimizer change.

Taken together, these appendix figures broaden the temporal evidence. Several measure families that depend directly on weight scale or spectrum—Frobenius norms, spectral surrogates, and parts of the PAC–Bayes suite—react strongly to an optimizer swap despite matching accuracy, while others such as margin-based quantities and the VC proxy remain largely stable. Reading these results in aggregate helps separate measure-intrinsic behavior from optimizer-driven drift and, with the log-time view, clarifies whether apparent motion reflects genuine multiplicative change or merely late-stage additive updates. For temporal behavior of path norms, see Section 4, where those panels are discussed in detail.

C. Proof for theorem 6.2

In this section we prove Theorem 6.2. We first reintroduce the scale invariance lemma from Arora et al. (2018b); Li & Arora (2019) which is the key source of intuition about scale-invariant networks.

Lemma C.1 (Scale-invariant networks). *If $\forall c \in \mathbb{R}^+$, $L(\boldsymbol{\theta}) = L(c\boldsymbol{\theta})$, then*

1. $\langle \nabla_{\boldsymbol{\theta}} L, \boldsymbol{\theta} \rangle = 0$
2. $\nabla_{\boldsymbol{\theta}} L|_{\boldsymbol{\theta}=\boldsymbol{\theta}_0} = c \nabla_{\boldsymbol{\theta}} L|_{\boldsymbol{\theta}=c\boldsymbol{\theta}_0}$, for any $c > 0$

Proof. Treat c as a differentiable variable. Clearly the derivative of L w.r.t. c is 0.

$$1. 0 = \frac{\partial L}{\partial c} = \langle \nabla_{\boldsymbol{\theta}} L, \boldsymbol{\theta} \rangle$$

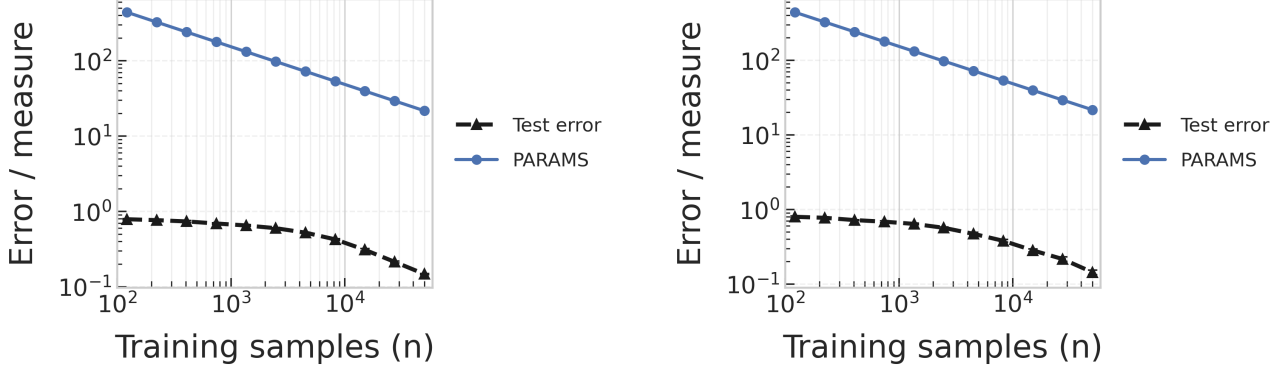


Figure S9. VC-dimension proxy, ResNet-50 on CIFAR-10 (Adam). Left: $\eta=10^{-3}$; right: $\eta=10^{-2}$. Nearly identical monotone decays; a useful control.

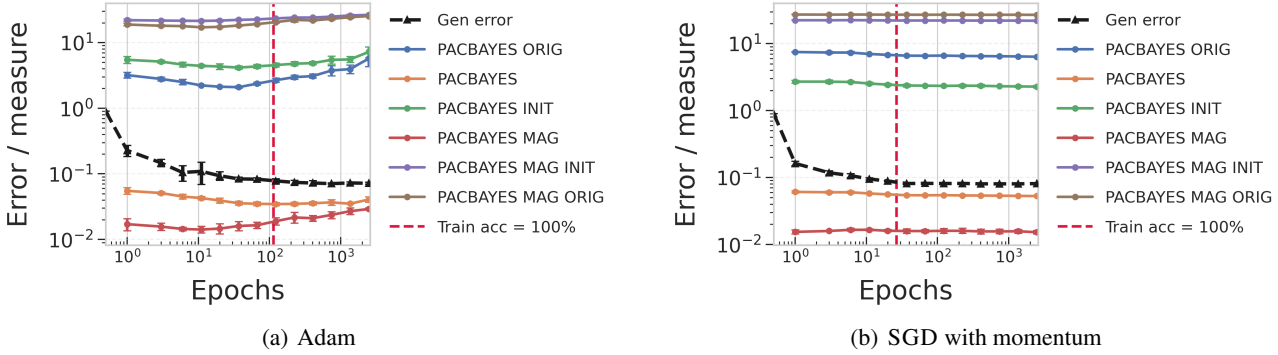


Figure S10. Temporal behavior for PAC–Bayes variants on ResNet–50/FashionMNIST at fixed learning rate 0.01. The epoch axis is logarithmic and the red dashed vertical line marks the first 100% training-accuracy epoch. ADAM exhibits slow post-accuracy growth (notably in PACBAYES_ORIG and PACBAYES_INIT), whereas SGD with momentum keeps the family flat once the dashed line is crossed.

2. Take gradient of the both sides of the equation $L(\boldsymbol{\theta}) = L(c\boldsymbol{\theta})$ w.r.t. $\boldsymbol{\theta}$ and set $\boldsymbol{\theta} = \boldsymbol{\theta}_0$, we immediately arrive at the result.

□

We give the technical definition of the commonly used training algorithm SGD with momentum and weight decay (WD) (with respect to the L2 norm of the parameters) using a convenient form given in Li & Arora (2019), which is equivalent to the default implementation in Pytorch (Paszke et al., 2017).

Definition C.2 (SGD with momentum and WD). At iteration t , given the current parameters and learning rate $(\boldsymbol{\theta}_{t-1}, \eta_{t-1})$, the buffered parameters and learning rate $(\boldsymbol{\theta}_{t-2}, \eta_{t-2})$, momentum factor γ , current loss $L(\boldsymbol{\theta}_{t-1})$ and WD factor λ_{t-1} , update the parameters $\boldsymbol{\theta}_t$ as the following:

$$\frac{\boldsymbol{\theta}_t - \boldsymbol{\theta}_{t-1}}{\eta_{t-1}} = \gamma \frac{\boldsymbol{\theta}_{t-1} - \boldsymbol{\theta}_{t-2}}{\eta_{t-2}} - \nabla_{\boldsymbol{\theta}} \left(L(\boldsymbol{\theta}_{t-1}) + \frac{\lambda_{t-1}}{2} \|\boldsymbol{\theta}_{t-1}\|_2^2 \right) \quad (21)$$

For the boundary conditions, it is a common practice to set $\boldsymbol{\theta}_{-1} = \boldsymbol{\theta}_0$ and η_{-1} can be arbitrary.

From the above definition, it is easy to see that we can represent the state of the algorithm using a four-tuple $(\boldsymbol{\theta}, \eta, \boldsymbol{\theta}', \eta')$, which stand for the parameters/learning rate at the current step and their buffers from the last step, respectively. A gradient descent step at time t with momentum factor γ and WD factor λ can be seen as a mapping between two states:

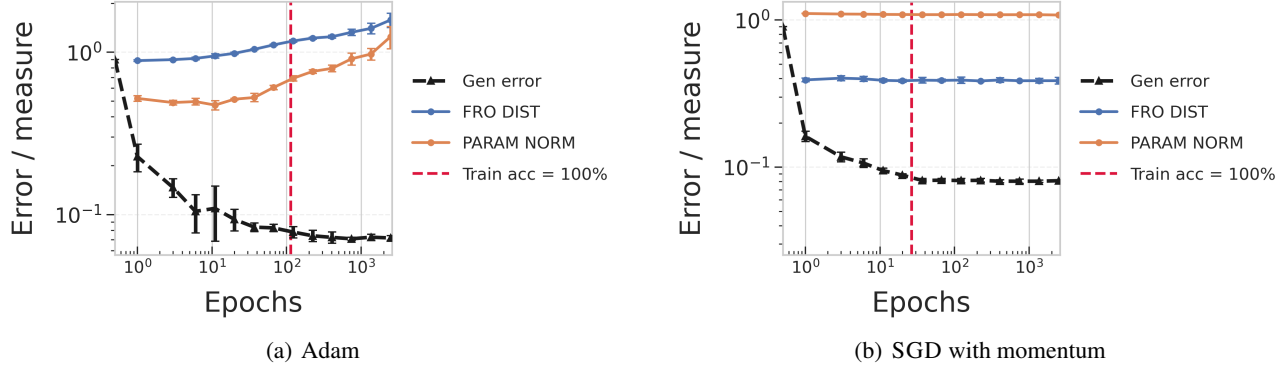


Figure S11. Frobenius distance and parameter norm through time. The epoch axis is logarithmic. ADAM produces continued growth in both FRO_DIST and PARAM_NORM after 100% training accuracy, while SGD with momentum holds them near a constant level.

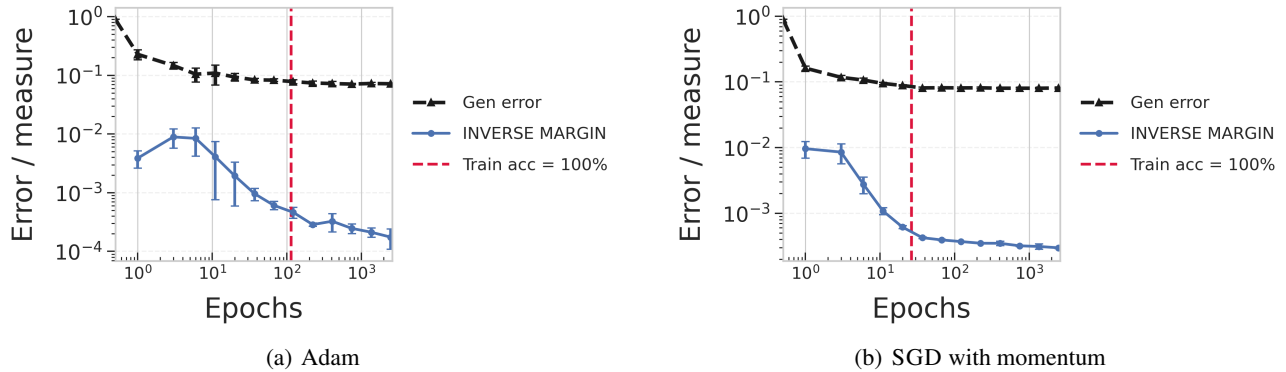


Figure S12. Inverse-margin surrogate through time on a logarithmic epoch axis. Both optimizers shrink the measure quickly and then hover near a floor; ADAM stabilizes at a slightly higher level but the overall shape is shared.

- A GD step with momentum and WD: $\text{GD}_t^\rho(\boldsymbol{\theta}, \eta, \boldsymbol{\theta}', \eta') = \left(\rho\boldsymbol{\theta} + \eta \left(\gamma \frac{\boldsymbol{\theta} - \boldsymbol{\theta}'}{\eta'} - \nabla L(\boldsymbol{\theta}) \right), \eta, \boldsymbol{\theta}, \eta \right)$

Here with WD factor being λ , ρ is set to be $1 - \lambda\eta$. Furthermore, we define some extra basic mappings that can be composed together to represent the temporal behavior of the algorithm.

- Scale current parameters $\boldsymbol{\theta}$: $\Pi_1^c(\boldsymbol{\theta}, \eta, \boldsymbol{\theta}', \eta') = (c\boldsymbol{\theta}, \eta, \boldsymbol{\theta}', \eta');$
- Scale current LR η : $\Pi_2^c(\boldsymbol{\theta}, \eta, \boldsymbol{\theta}', \eta') = (\boldsymbol{\theta}, c\eta, \boldsymbol{\theta}', \eta');$
- Scale buffered parameter $\boldsymbol{\theta}'$: $\Pi_3^c(\boldsymbol{\theta}, \eta, \boldsymbol{\theta}', \eta') = (\boldsymbol{\theta}, \eta, c\boldsymbol{\theta}', \eta');$
- Scale buffered LR η' : $\Pi_4^c(\boldsymbol{\theta}, \eta, \boldsymbol{\theta}', \eta') = (\boldsymbol{\theta}, \eta, \boldsymbol{\theta}', c\eta').$

We know that in scale-invariant neural nets, two networks $f(\boldsymbol{\theta})$ and $f(\tilde{\boldsymbol{\theta}})$ are equivalent if $\exists c > 0$ such that $\tilde{\boldsymbol{\theta}} = c\boldsymbol{\theta}$; Here we extend the equivalence between weights to the equivalence between states of algorithms:

Definition C.3 (Equivalent states). Two states $(\boldsymbol{\theta}, \eta, \boldsymbol{\theta}', \eta')$ and $(\tilde{\boldsymbol{\theta}}, \tilde{\eta}, \tilde{\boldsymbol{\theta}'}, \tilde{\eta}')$ are *equivalent* iff $\exists c > 0$ such that $(\boldsymbol{\theta}, \eta, \boldsymbol{\theta}', \eta') = [\Pi_1^c \circ \Pi_2^{c^2} \circ \Pi_3^c \circ \Pi_4^{c^2}] (\tilde{\boldsymbol{\theta}}, \tilde{\eta}, \tilde{\boldsymbol{\theta}'}, \tilde{\eta}') = (c\tilde{\boldsymbol{\theta}}, c^2\tilde{\eta}, c\tilde{\boldsymbol{\theta}'}, c^2\tilde{\eta}')$, which is also noted as $(\boldsymbol{\theta}, \eta, \boldsymbol{\theta}', \eta') \stackrel{c}{\sim} (\tilde{\boldsymbol{\theta}}, \tilde{\eta}, \tilde{\boldsymbol{\theta}'}, \tilde{\eta}')$. We call $[\Pi_1^c \circ \Pi_2^{c^2} \circ \Pi_3^c \circ \Pi_4^{c^2}]$ as *equivalent scaling* for all $c > 0$.

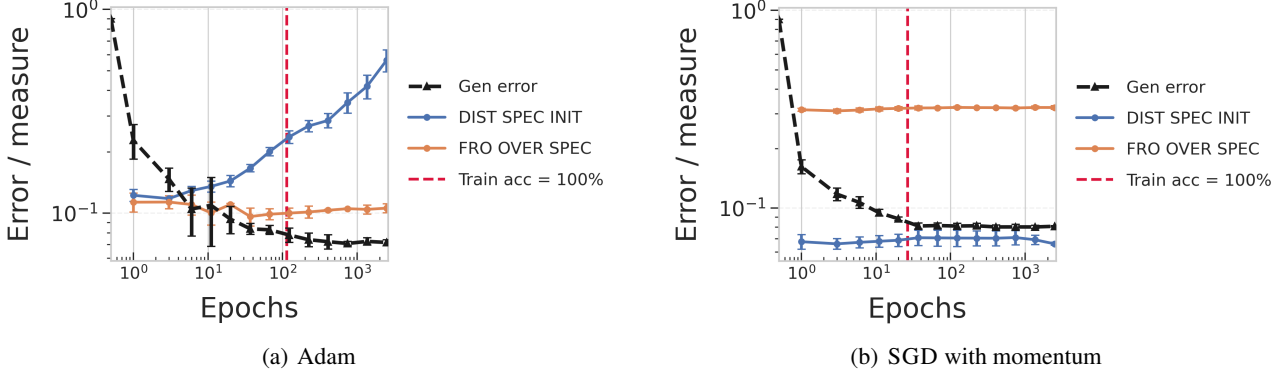


Figure S13. Spectral metrics through time. The epoch axis is logarithmic. ADAM drives DIST_SPEC_INIT upward after interpolation, while momentum SGD yields a gentle decline; FRO_OVER_SPEC diverges slightly in level.

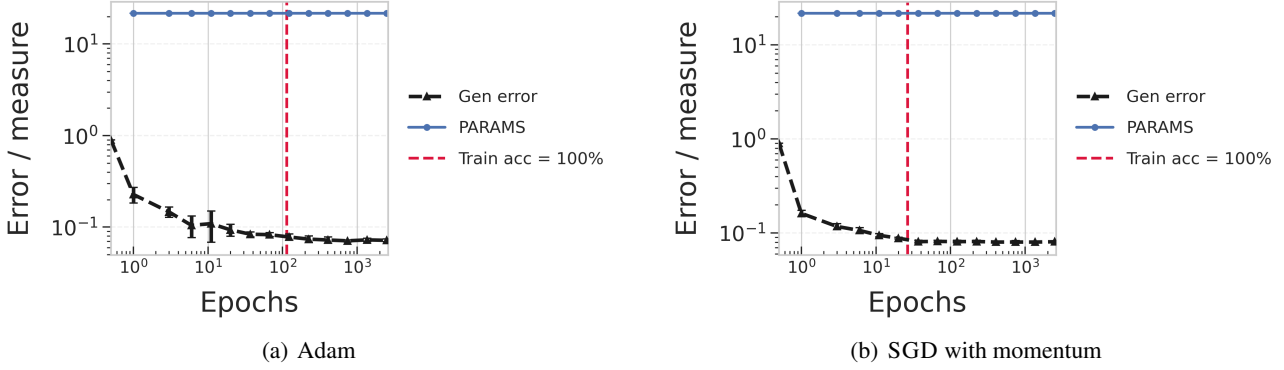


Figure S14. VC-dimension proxy and generalization error through time on a logarithmic epoch axis. The parameter-count surrogate is identical for both optimizers and the error trajectories are similarly calm, providing a neutral reference.

Here we provide an intuitive explanation of why the equivalent scaling takes the form above. If we rearrange the first term of the R.H.S. of the GD update, and assume we are operating in a regime where $\eta' = \eta^1$, we have

$$\theta_{\text{update}} = (\rho + \gamma)\theta - \eta \nabla L(\theta) - \gamma \theta' \quad (22)$$

In order to keep the updated parameters in the same direction, the three terms in equation 22 need to have the same scaling. From lemma C.1 we know that when θ is scaled by c , the gradient $\nabla L(\theta)$ will actually be scaled by $\frac{1}{c}$. Hence for the second term $\eta \nabla L(\theta)$ to have the same amount of scaling as the first and third terms, η has to be scaled by c^2 .

The following lemma tells us that equivalent scaling commutes with GD update with momentum and WD, implying that equivalence is preserved under GD updates. Hence we are free to stack GD updates and insert equivalent scaling anywhere in a sequence of basic maps without changing the network function.

Lemma C.4 (Equivalent scaling commutes with GD). $\forall c, \rho > 0$ and $t \geq 0$,

$$GD_t^\rho \circ \left[\Pi_1^c \circ \Pi_2^{c^2} \circ \Pi_3^c \circ \Pi_4^{c^2} \right] = \left[\Pi_1^c \circ \Pi_2^{c^2} \circ \Pi_3^c \circ \Pi_4^{c^2} \right] \circ GD_t^\rho.$$

In other words, if $(\theta, \eta, \theta', \eta') \stackrel{c}{\sim} (\tilde{\theta}, \tilde{\eta}, \tilde{\theta}', \tilde{\eta}')$ then $GD_t^\rho(\theta, \eta, \theta', \eta') \stackrel{c}{\sim} GD_t^\rho(\tilde{\theta}, \tilde{\eta}, \tilde{\theta}', \tilde{\eta}')$.

¹This just means in the eyes of the GD algorithm, the buffered LR and the current LR are the same. It does not exclude the possibility that we can still scale the current LR between GD updates.

Proof. For any given state $(\boldsymbol{\theta}, \eta, \boldsymbol{\theta}', \eta')$, the L.H.S. of the equation is:

$$\begin{aligned}
 \text{GD}_t^\rho \circ \left[\Pi_1^c \circ \Pi_2^{c^2} \circ \Pi_3^c \circ \Pi_4^{c^2} \right] (\boldsymbol{\theta}, \eta, \boldsymbol{\theta}', \eta') &= \text{GD}_t^\rho(c\boldsymbol{\theta}, c^2\eta, c\boldsymbol{\theta}', c^2\eta') \\
 &= \left(\rho c\boldsymbol{\theta} + c^2\eta \left(\gamma \frac{c\boldsymbol{\theta} - c\boldsymbol{\theta}'}{c^2\eta'} - \nabla L(c\boldsymbol{\theta}) \right), c^2\eta, c\boldsymbol{\theta}, c^2\eta \right) \\
 &= \left(c \left(\rho\boldsymbol{\theta} + \eta \left(\gamma \frac{\boldsymbol{\theta} - \boldsymbol{\theta}'}{\eta'} - \nabla L(\boldsymbol{\theta}) \right) \right), c^2\eta, c\boldsymbol{\theta}, c^2\eta \right) \\
 &= \left[\Pi_1^c \circ \Pi_2^{c^2} \circ \Pi_3^c \circ \Pi_4^{c^2} \right] \circ \text{GD}_t^\rho(\boldsymbol{\theta}, \eta, \boldsymbol{\theta}', \eta')
 \end{aligned}$$

□

Now comes the important step: in order to show the equivalence between two series of parameters with (fixed WD + fixed LR)/(exponentially decreasing WD + exponentially increasing LR), respectively, we need to rewrite GD_t^ρ as a composition of itself with varying WD factor and upscaling LR, conjugated with other scaling terms that cancel with each other eventually. Here again we choose to work in the regime where the current and buffered LR are the same in the input of GD_t^ρ .

Lemma C.5 (Conjugated GD updates). *For any input with equal current and buffered LR $(\boldsymbol{\theta}, \eta, \boldsymbol{\theta}', \eta)$ and $\forall \alpha \in (Z_0, Z_1] \cup [Z_2, 1)$ ², we have*

$$\text{GD}_t^\rho(\boldsymbol{\theta}, \eta, \boldsymbol{\theta}', \eta) = \left[\Pi_4^\alpha \circ \Pi_2^\alpha \circ \Pi_1^\alpha \circ \text{GD}_t^\beta \circ \Pi_2^{\alpha^{-1}} \circ \Pi_3^\alpha \circ \Pi_4^\alpha \right] (\boldsymbol{\theta}, \eta, \boldsymbol{\theta}', \eta)$$

which can be written in the form of equivalent states:

$$\text{GD}_t^\rho(\boldsymbol{\theta}, \eta, \boldsymbol{\theta}', \eta) \underset{\alpha}{\sim} \left[\Pi_3^{\alpha^{-1}} \circ \Pi_4^{\alpha^{-1}} \circ \Pi_2^{\alpha^{-1}} \circ \text{GD}_t^\beta \circ \Pi_2^{\alpha^{-1}} \circ \Pi_3^\alpha \circ \Pi_4^\alpha \right] (\boldsymbol{\theta}, \eta, \boldsymbol{\theta}', \eta) \quad (23)$$

where

- $\beta = \frac{(\rho+\gamma)}{\alpha} - \frac{\gamma}{\alpha^2}$
- $Z_0 = \frac{\gamma}{1-\lambda\eta_0+\gamma}$
- $Z_1 = \frac{1+\gamma-\lambda\eta_0-\sqrt{(1-\gamma)^2-2(1+\gamma)\lambda\eta_0+\lambda^2\eta_0^2}}{2}$
- $Z_2 = \frac{1+\gamma-\lambda\eta_0+\sqrt{(1-\gamma)^2-2(1+\gamma)\lambda\eta_0+\lambda^2\eta_0^2}}{2}$ ³

Proof. We directly verify the equivalence. The R.H.S. is:

$$\begin{aligned}
 &\left[\Pi_4^\alpha \circ \Pi_2^\alpha \circ \Pi_1^\alpha \circ \text{GD}_t^\beta \circ \Pi_2^{\alpha^{-1}} \circ \Pi_3^\alpha \circ \Pi_4^\alpha \right] (\boldsymbol{\theta}, \eta, \boldsymbol{\theta}', \eta) \\
 &= [\Pi_4^\alpha \circ \Pi_2^\alpha \circ \Pi_1^\alpha] \circ \text{GD}_t^\beta(\boldsymbol{\theta}, \alpha^{-1}\eta, \alpha\boldsymbol{\theta}', \alpha\eta) \\
 &= [\Pi_4^\alpha \circ \Pi_2^\alpha \circ \Pi_1^\alpha] \left(\beta\boldsymbol{\theta} + \alpha^{-1}\eta \left(\gamma \frac{\boldsymbol{\theta} - \alpha\boldsymbol{\theta}'}{\alpha\eta} - \nabla L(\boldsymbol{\theta}) \right), \alpha^{-1}\eta, \boldsymbol{\theta}, \alpha^{-1}\eta \right) \\
 &= \left(\alpha\beta\boldsymbol{\theta} + \eta \left(\gamma \frac{\boldsymbol{\theta} - \alpha\boldsymbol{\theta}'}{\alpha\eta} - \nabla L(\boldsymbol{\theta}) \right), \eta, \boldsymbol{\theta}, \eta \right) \\
 &= ((\rho + \gamma)\boldsymbol{\theta} - \gamma\boldsymbol{\theta}' - \eta\nabla L(\boldsymbol{\theta}), \eta, \boldsymbol{\theta}, \eta) \\
 &= \left(\rho\boldsymbol{\theta} + \eta \left(\gamma \frac{\boldsymbol{\theta} - \boldsymbol{\theta}'}{\eta} - \nabla L(\boldsymbol{\theta}) \right), \eta, \boldsymbol{\theta}, \eta \right) \\
 &= \text{GD}_t^\rho(\boldsymbol{\theta}, \eta, \boldsymbol{\theta}', \eta)
 \end{aligned}$$

The range of α can be easily shown by combining the following two constraints and assuming remark 6.3 is true:

²Technically α can be larger than 1, but in that case we will be shrinking the LR between GD steps which is not what we mainly care about here.

³It's easy to verify that Z_2 is always smaller than 1.

- $\alpha \in (0, 1]$;
- $\frac{(\rho+\gamma)}{\alpha} - \frac{\gamma}{\alpha^2} \in (0, 1]$

□

Now we are ready to prove theorem 6.2.

Proof of Theorem 6.2. From the assumption we have the following equivalence between the boundary conditions of the two series of states:

$$\begin{aligned} (\boldsymbol{\theta}_0, \eta_0, \boldsymbol{\theta}_{-1}, \eta_{-1}) &= (\boldsymbol{\theta}_0, \eta_0, \boldsymbol{\theta}_0, \eta_0) \\ (\tilde{\boldsymbol{\theta}}_0, \tilde{\eta}_0, \tilde{\boldsymbol{\theta}}_{-1}, \tilde{\eta}_{-1}) &= \left[\Pi_2^{\alpha^{-1}} \circ \Pi_3^{\alpha} \circ \Pi_4^{\alpha} \right] (\boldsymbol{\theta}_0, \eta_0, \boldsymbol{\theta}_{-1}, \eta_{-1}) \end{aligned}$$

Lemma C.4 tells us that equivalent states are still equivalent after both being transformed by a GD step. Hence we can stack up on both sides of equation 23 for a finite number of times. i.e. for $\forall t \geq 0$, we have

$$\begin{aligned} &\text{GD}_{t-1}^{\rho} \circ \text{GD}_{t-2}^{\rho} \circ \cdots \circ \text{GD}_0^{\rho} (\boldsymbol{\theta}_0, \eta_0, \boldsymbol{\theta}_{-1}, \eta_{-1}) \\ &\stackrel{\alpha^t}{\sim} \left[\Pi_3^{\alpha^{-1}} \circ \Pi_4^{\alpha^{-1}} \circ \Pi_2^{\alpha^{-1}} \circ \text{GD}_{t-1}^{\beta} \circ \Pi_2^{\alpha^{-1}} \circ \Pi_3^{\alpha} \circ \Pi_4^{\alpha} \right] \\ &\quad \circ \cdots \circ \left[\Pi_3^{\alpha^{-1}} \circ \Pi_4^{\alpha^{-1}} \circ \Pi_2^{\alpha^{-1}} \right] \circ \text{GD}_0^{\beta} (\tilde{\boldsymbol{\theta}}_0, \tilde{\eta}_0, \tilde{\boldsymbol{\theta}}_{-1}, \tilde{\eta}_{-1}) \\ &\stackrel{\alpha^t}{\sim} \left[\Pi_3^{\alpha^{-1}} \circ \Pi_4^{\alpha^{-1}} \circ \Pi_2^{\alpha^{-1}} \circ \text{GD}_{t-1}^{\beta} \circ \Pi_2^{\alpha^{-2}} \circ \text{GD}_{t-2}^{\beta} \circ \cdots \circ \Pi_2^{\alpha^{-2}} \circ \text{GD}_0^{\beta} \right] (\tilde{\boldsymbol{\theta}}_0, \tilde{\eta}_0, \tilde{\boldsymbol{\theta}}_{-1}, \tilde{\eta}_{-1}) \end{aligned}$$

which implies that

- $\boldsymbol{\theta}_t = \alpha^t \tilde{\boldsymbol{\theta}}_t$
- $\tilde{\eta}_t = \alpha^{-2t} \tilde{\eta}_0 = \alpha^{-2t-1} \eta_0$
- $\tilde{\lambda}_t = \frac{1-\beta}{\tilde{\eta}_t}$, except for $t = 0$, in which case $\tilde{\lambda}_0 = \frac{1-\beta + \frac{\gamma}{\alpha^2} - \frac{\gamma}{\alpha}}{\tilde{\eta}_0}$

We note the special boundary condition for $\tilde{\lambda}_0$ due to the fact that $\tilde{\boldsymbol{\theta}}_{-1} \neq \tilde{\boldsymbol{\theta}}_0$. □

D. Additional label-corruption results: PAC–Bayes and Path Norms

This appendix gathers the label–corruption results referenced in the main text for both PAC–Bayes–style measures and Path Norms.

PAC–Bayes measures. Under ADAM, lowering the learning rate from 10^{-2} to 10^{-3} transforms a clean, steadily rising ramp (e.g., PACBAYES_ORIG from ~ 3.6 past 4.7) into a higher–lying but *shallower* U–shape centred around ~ 8 . At fixed learning rate 10^{-2} , swapping ADAM for SGD produces a striking level shift: SGD yields a *high plateau* (~ 12 –13) with little curvature, while ADAM traces a *low*, clearly increasing arc (~ 3.6 –4.7). Even within the PAC–Bayes family, members respond differently by optimizer: PACBAYES_INIT grows aggressively under ADAM but only mildly under SGD. These patterns illustrate an (often) *insensitive* or contradictory relationship between the measure and increasing label corruption—another facet of fragility.

Path norms under SGD (momentum). Mirroring the Adam case in the main text, SGD with momentum exhibits an equally striking flip (Fig. S17): at $\text{LR}=10^{-3}$, the path-norm trajectory lives in the 10^4 – 10^5 band and *decays* steadily with corruption; at $\text{LR}=10^{-1}$, the scale *crashes* to nearly zero and the curve *climbs* monotonically. Trend and scale both invert. If a reader tried to infer “harder data \Rightarrow larger path norm” from one panel, the other would immediately contradict it.

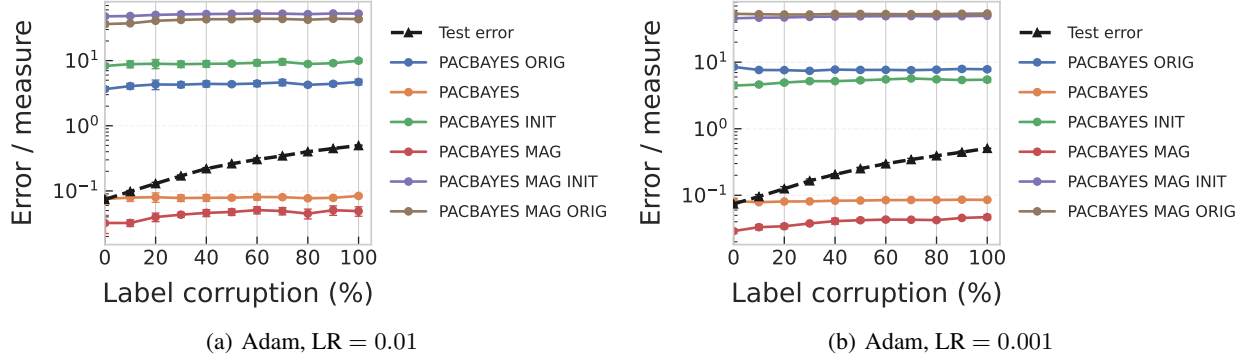


Figure S15. PAC–Bayes measures vs. label corruption under Adam. With $LR=10^{-2}$, the family rises steadily with corruption; with $LR=10^{-3}$ it sits higher overall and shows a shallow U–shape. All panels use 10,000 training samples.

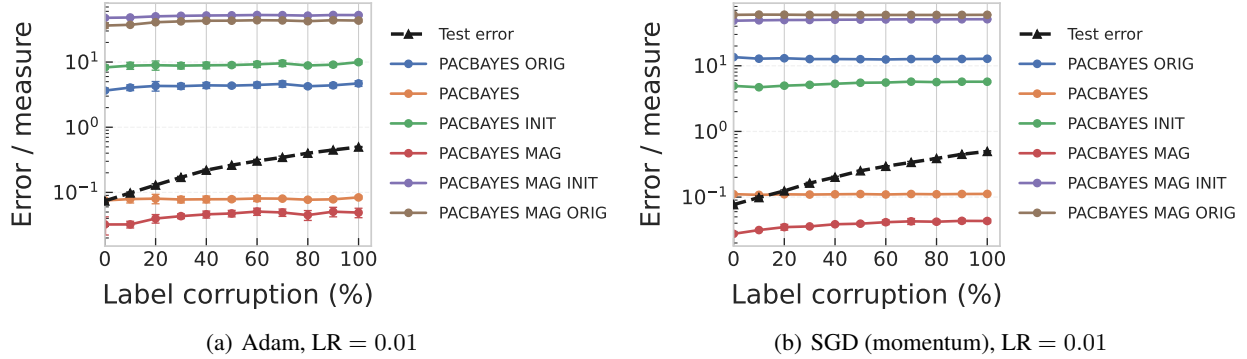


Figure S16. PAC–Bayes measures vs. label corruption at fixed $LR (10^{-2})$, swapping only the optimizer. Adam yields a low, steadily rising family (e.g., $PACBAYES_ORIG \approx 3.6\text{--}4.7$), whereas SGD holds a high plateau ($\sim 12\text{--}13$) with minimal curvature; $PACBAYES_INIT$ grows far more under ADAM than under SGD. All panels use 10,000 training samples.

E. Quantitative fragility: detailed results

This appendix extends Section 7. We first summarize the experimental setup, and then give concise, implementable procedures for our two instability scores: *CMS* and its seed-adjusted variant *eCMS*. We close with a brief reading guide that highlights what can be learned from the summary tables at Table 1 ($\delta = 0.01$), Table 2 ($\delta = 0.02$), and Table 3 ($\delta = 0.05$). For full definitions of the measures listed in those tables, see (Dziugaite et al., 2020b).

Experimental setup. We study two datasets—FASHIONMNIST and CIFAR-10—across three architectures: NETWORK-IN-NETWORK (NiN) (Lin et al., 2013), RESNET-50 (RN50), and DENSENET-121 (DN121). The training pipeline varies along three axes: (i) learning rate $lr \in \{0.001, 0.0032, 0.0063, 0.01, 0.0158, 0.05, 0.1\}$; (ii) optimizer $\in \{\text{ADAM}, \text{SGD} + \text{MOMENTUM}\}$; and (iii) stopping criterion: either the first epoch reaching 100% training accuracy, or the first epoch whose training cross-entropy drops below 0.01. Each hyperparameter configuration is replicated with 8 random seeds. We compute scores within each (dataset, architecture) group at absolute error tolerances $\delta \in \{0.01, 0.02, 0.05\}$, using natural logs and reporting medians.

Using the procedures in practice. Algorithms 1 and 2 specify the exact pair-construction and aggregation steps used throughout our study. In all tables, we apply these procedures within each (dataset, architecture) group and then report group-level medians; if a required pair set is empty for a group, the statistic is marked UNDEFINED and the group is omitted from the across-group aggregation. When the number of eligible pairs is large, we uniformly subsample up to a fixed budget K before taking the median, following the same steps as in Algorithms 1–2.

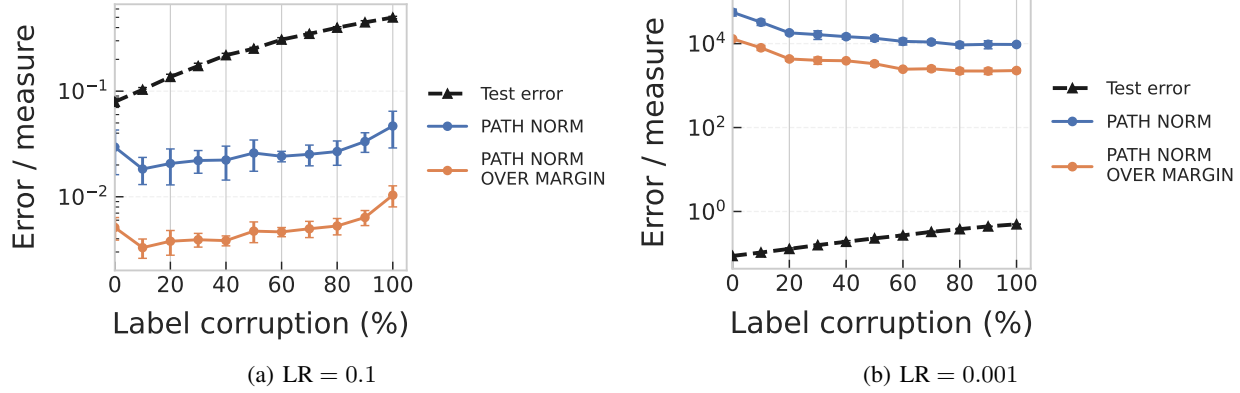


Figure S17. **Path norms vs. label corruption** with SGD (momentum); panels differ only in learning rate. At $LR=10^{-3}$ the curve sits in 10^4 – 10^5 and decays with corruption; at $LR=10^{-1}$ it lives near zero and rises. Both the direction and the dynamic range flip—another instance of qualitative mismatch across a minimal training change. *All panels use 10,000 training samples.*

Algorithm 1 CMS (Conditional Measure Spread)

Require: Runs $\{(C_r, \hat{\varepsilon}_r)\}_{r=1}^n$ with $C_r > 0$; tolerance $\delta > 0$; optional pair budget K .

Ensure: $CMS_\delta(C; g)$ for group g .

```

1: Sort indices so that  $\hat{\varepsilon}_{(1)} \leq \dots \leq \hat{\varepsilon}_{(n)}$ .
2:  $L \leftarrow []$  {container of  $|\log C - \log C'|$ }
3: for  $i \leftarrow 1$  to  $n$  do
4:    $j \leftarrow i + 1$ 
5:   while  $j \leq n$  and  $\hat{\varepsilon}_{(j)} - \hat{\varepsilon}_{(i)} \leq \delta$  do
6:     append  $|\log C_{(i)} - \log C_{(j)}|$  to  $L$ 
7:      $j \leftarrow j + 1$ 
8: if  $|L| = 0$  then return UNDEFINED {no close-error pairs}
9: if  $|L| > K$  then
10:   uniformly subsample  $K$  elements of  $L$ 
11: return median( $L$ )

```

What the tables show. The summaries in Table 1, Table 2, and Table 3 reveal clear, consistent patterns:

- **Stable control.** The parameter-count proxy (PARAMS) is uniformly flat ($CMS = 0$, $eCMS = 0$) across datasets, architectures, and tolerances; see the first row of Table 1 and its counterparts at $\delta = 0.02$ and $\delta = 0.05$.
- **PAC–Bayes surrogates split.** The classical parameter-space PACBAYES_ORIG exhibits substantial instability (elevated CMS and $eCMS$), often increasing as the tolerance widens (compare the “ORIG” rows across Tables 1 and 2). Magnitude-aware variants (e.g., PACBAYES_MAG_*) are consistently lower, though they remain sensitive on FASHIONMNIST with deeper architectures.
- **Norm families are fragile.** Parameter and path norms already show sizeable spreads at $\delta = 0.01$ and inflate further at $\delta = 0.02$ – 0.05 . Frobenius and spectral *distances from initialization* are larger still and consistently among the most unstable rows across tables.
- **Product/aggregate spectral–Frobenius measures are outliers.** Aggregate/product metrics (e.g., LOG_PROD_OF_SPEC, LOG_SPEC_*) and Frobenius analogues exhibit spreads that are orders of magnitude larger than other families at $\delta = 0.01$, and this gap persists at $\delta = 0.02$ and $\delta = 0.05$.
- **Beyond seeds.** For many families (e.g., PACBAYES_ORIG, PARAM_NORM, FRO_DIST) we observe $eCMS > CMS$ across tolerances, indicating that a substantial portion of the jumpiness is attributable to hyperparameter changes rather than random seeds; exceptions exist for specific (dataset, architecture) cells.
- **Where fragility concentrates.** Per-group columns indicate that the largest spreads tend to cluster on FASHIONMNIST with RN50/DN121, while CIFAR-10/NIN often shows the smallest values for the same measure (compare group

Algorithm 2 eCMS (seed-adjusted CMS)

Require: Runs $\{(C_r, \hat{\varepsilon}_r, H_r, \text{seed}_r)\}_{r=1}^n$ with $C_r > 0$; tolerance $\delta > 0$; optional pair budget K .

Ensure: $\text{eCMS}_\delta(C; g) = [\text{CMS}_\delta^{\text{inter}} - \text{CMS}_\delta^{\text{seed}}]_+$ for g .

```

1: Sort indices so that  $\hat{\varepsilon}_{(1)} \leq \dots \leq \hat{\varepsilon}_{(n)}$ .
2:  $L_{\text{seed}} \leftarrow []$ ,  $L_{\text{inter}} \leftarrow []$ 
3: for  $i \leftarrow 1$  to  $n$  do
4:    $j \leftarrow i + 1$ 
5:   while  $j \leq n$  and  $\hat{\varepsilon}_{(j)} - \hat{\varepsilon}_{(i)} \leq \delta$  do
6:     if  $H_{(j)} = H_{(i)}$  and  $\text{seed}_{(j)} \neq \text{seed}_{(i)}$  then
7:       append  $|\log C_{(i)} - \log C_{(j)}|$  to  $L_{\text{seed}}$ 
8:     else if  $H_{(j)} \neq H_{(i)}$  then
9:       append  $|\log C_{(i)} - \log C_{(j)}|$  to  $L_{\text{inter}}$ 
10:     $j \leftarrow j + 1$ 
11: if  $|L_{\text{inter}}| = 0$  or  $|L_{\text{seed}}| = 0$  then return UNDEFINED
12: if  $|L_{\text{seed}}| > K$  then
13:   uniformly subsample  $K$  elements of  $L_{\text{seed}}$ 
14: if  $|L_{\text{inter}}| > K$  then
15:   uniformly subsample  $K$  elements of  $L_{\text{inter}}$ 
16:  $\text{CMS}_\delta^{\text{seed}} \leftarrow \text{median}(L_{\text{seed}})$ 
17:  $\text{CMS}_\delta^{\text{inter}} \leftarrow \text{median}(L_{\text{inter}})$ 
18: return  $\max\{0, \text{CMS}_\delta^{\text{inter}} - \text{CMS}_\delta^{\text{seed}}\}$ 

```

subcolumns across tables).

A note on scope. Our quantitative fragility scores target a single desideratum: *when test error does not change, a credible generalization measure should remain stable*. Scoring well on CMS/eCMS does *not* imply that a measure is “correct” or sufficient. For example, VC dimension/parameter count is widely regarded as a poor complexity measure for modern deep networks, yet it is not fragile in our sense (cf. PARAMS rows). Likewise, the ML-PACBayes bound discussed in the main text (§F) is not fragile largely because it is agnostic to hyperparameter changes. Stability is necessary for utility, but it is not, by itself, a full explanation of generalization.

F. Post-mortem vs. ML-PACBayes

We contrast post-training (“post-mortem”) generalization measures with a function-space approach based on the marginal-likelihood PAC–Bayes bound of [Valle-Pérez & Louis \(2020\)](#). The bound controls the test error of a hypothesis sampled from a Bayesian posterior over *functions* (not parameters); the key capacity term is the marginal likelihood (Bayesian evidence) of the data under the architecture’s Gaussian-process (GP) limit. **All figure numbers below refer to Valle-Pérez & Louis (2020).**

Definition F.1 (Marginal-likelihood PAC–Bayes bound). Consider binary classification with data distribution \mathcal{D} over $\mathcal{X} \times \{0, 1\}$ and a hypothesis space \mathcal{H} of functions $h : \mathcal{X} \rightarrow \{0, 1\}$. Let $S \sim \mathcal{D}^n$ be a training set of size $n \geq 2$, and let P be a prior on \mathcal{H} . Define the consistency set

$$C(S) := \{h \in \mathcal{H} : \hat{\varepsilon}(h, S) = 0\},$$

where $\hat{\varepsilon}(h, S) = \frac{1}{n} \sum_{(x,y) \in S} \mathbf{1}\{h(x) \neq y\}$ is the empirical 0–1 error. The (realizable) Bayesian posterior supported on $C(S)$ is

$$Q(h) = \begin{cases} \frac{P(h)}{P(C(S))}, & h \in C(S), \\ 0, & \text{otherwise,} \end{cases}$$

where $P(C(S)) = \sum_{h \in C(S)} P(h)$ is the *marginal likelihood* (Bayesian evidence) of S .

For any confidence levels $\delta, \gamma \in (0, 1]$, with probability at least $1 - \delta$ over $S \sim \mathcal{D}^n$ and, conditional on S , with probability

at least $1 - \gamma$ over $h \sim Q$, the generalization error $\varepsilon(h) = \Pr_{(x,y) \sim \mathcal{D}}[h(x) \neq y]$ satisfies

$$-\ln(1 - \varepsilon(h)) < \frac{\ln \frac{1}{P(C(S))} + \ln n + \ln \frac{1}{\delta} + \ln \frac{1}{\gamma}}{n - 1}. \quad (24)$$

Remark F.2 (binary vs. multiclass). We state the bound for binary classification for clarity; the function-space marginal-likelihood perspective extends to multiclass via standard reductions (e.g., one-vs-rest) or multiclass likelihoods.

What our fragility checks reveal—and what the ML-PACBayes bound gets right. We evaluated each measure against consequential perturbations: dataset difficulty, data-size scaling, training-pipeline changes, and temporal behavior (overtraining). Post-mortem measures (sharpness/flatness, norm/margin proxies, compression-style, and deterministic PAC–Bayes surrogates) often fail at least one stressor; in our runs, even strong performers such as PACBAYES_orig failed key tests. By contrast, the GP-based bound tracks the *function-level* regularities we care about:

- **Data complexity.** The marginal-likelihood bound *tracks dataset difficulty*: it increases with label corruption and preserves the canonical ordering MNIST < Fashion-MNIST < CIFAR-10; see Figure 1 in (Valle-Pérez & Louis, 2020). In our audits, several post-mortem measures—including PACBAYES_orig—either flattened under corruption or were not able to catch the ordering, even when the test error did.
- **Learning-curve scaling.** The marginal-likelihood bound *tracks learning-curve scaling*: it mirrors the empirical power-law in n and clusters exponents primarily by *dataset*; see Figures 2–5 in (Valle-Pérez & Louis, 2020). By contrast, some post-mortem measures barely moved with n ; others bent the wrong way or mixed optimizer effects with data effects (cf. (Nagarajan & Kolter, 2019)).
- **Temporal behavior (overtraining invariance).** The marginal-likelihood bound *tracks temporal invariance*: once S is fixed and training has interpolated ($\hat{\varepsilon} = 0$), the bound depends only on $P(C(S))$ and n —it is agnostic to how long or by which path the parameters were trained. In our temporal-behavior experiments, several norm-based post-mortem measures (e.g., ℓ_2 /spectral/path norms) *kept growing* during overtraining while the generalization error stayed roughly unchanged; the GP bound remained stable. (This echoes broader observations that longer training can leave test error flat or improved (Hoffer et al., 2017), and that norms can diverge under separable losses without hurting classification error (Soudry et al., 2018).)
- **Training-pipeline changes.** Many post-mortem measures swing with optimizer, batch size, explicit/implicit regularization, and early stopping—sometimes tracking curvature artifacts rather than out-of-sample error (e.g., Keskar et al., 2017; Hochreiter & Schmidhuber, 1997; Jiang et al., 2019b; Dziugaite et al., 2020b). The GP marginal-likelihood bound is, by construction, insensitive to these knobs: it depends on the architecture’s function prior and the data, not on the path taken through parameter space. We view this *invariance* as a virtue for a predictor; the bound is not designed to explain *differences caused by* optimizer choice and should not be judged on that criterion.

These properties are consistent with our optimizer-swap and pixel-permutation stress tests (Apps. B and G) and with our scale-symmetry Exp++ dial, which only alters parameter scale (App. H).

Why does the function-space route outperform post-mortems? Two ingredients stand out. First, the bound evaluates an Occam factor in *function space*: architectures that place high prior mass on data-compatible functions earn better evidence, naturally capturing dataset ordering and learning-curve slopes. Second, there is a credible external yardstick: infinite-width GP predictors (NNGP/NTK) often *quantitatively* predict finite-width DNN generalization trends (Lee et al., 2020a). Together, these explain why Figures 1–5 show greater stability for the GP-based approach than we observe for post-hoc, parameter-space measures.

So why do post-mortems underperform? The live hypothesis is that they *measure the wrong object*. Post-mortem scores probe properties of a single trained parameter vector (curvature, norms, compressibility), entangling optimization details and reparameterization choices with generalization. That enterprise is important—and the community has argued forcefully that such post-training diagnostics deserve attention (e.g., compression and robustness perspectives in Arora et al., 2018a; 2019; Jiang et al., 2019b; Dziugaite et al., 2020b)—but our evidence suggests their predictions are fragile under routine perturbations. By contrast, the GP bound targets the distribution over *functions* implied by architecture and data.

Open question. Even if the GP-based predictor/bound wins these stress tests, finite-width networks can outperform their GP limits; yet the GP still predicts a striking fraction of performance trends (Figures 2–5). Closing this gap—by designing reparameterization-invariant, data-aware post-mortem diagnostics that inherit the Occam flavour of marginal likelihood—remains open.

G. Stress-testing generalization measures with pixel permutations

A useful generalization measure should pass two basic stress tests: (i) it should be *insensitive* to symmetry-preserving transformations that do not change the intrinsic task, yet (ii) *sensitive* when task-relevant information is destroyed. Pixel permutations provide such a testbed: applying the *same* permutation to the training and test sets preserves label–input relationships (a symmetry for fully connected networks), whereas applying *independent* random permutations to train and test destroys spatial structure and any usable signal.

We evaluate three families of measures alongside test error on MNIST with two architectures: a fully connected network (FCN) and a ResNet-50. We vary the optimizer (SGD vs. ADAM) and the early-stopping criterion (best cross-entropy “CE” vs. best accuracy “Acc”) to expose hyperparameter sensitivity. Results are summarized in Tables 4 and 5.

FCN (permutation symmetry holds). When the same pixel permutation is applied to both train and test, the FCN effectively sees an unchanged task. As expected, test error remains essentially constant (≈ 0.03 across optimizers/stopping), and the PAC-Bayesian marginal likelihood (ML) bound is flat (0.142 throughout). This indicates desirable *robustness* to symmetry-preserving changes. In contrast, under independent random permutations, test error rises to ≈ 0.49 –0.50 (near random guessing), and the ML bound increases to 0.532—appropriately reflecting reduced learnability. The path norm and the original PAC-Bayes variant (PACBAYES-ORIG) trend upward in this harder setting, but they also exhibit large spread across optimizers/stopping; e.g., the path norm spans from 0.105 to 6.632 under random shuffling, smaller than some unshuffled cases, revealing *fragility* to seemingly minor training choices.

ResNet-50 (permutation symmetry broken). Because convolutional inductive biases depend on spatial locality, even a single shared permutation distorts the data geometry and degrades performance (test error increases from ≈ 0.014 –0.025 to ≈ 0.041 –0.060; the ML bound rises from 0.101 to 0.170). With independent random permutations, test error again moves to ≈ 0.44 –0.46 and the ML bound to ≈ 0.504 . The path norm is particularly volatile here, spanning *orders of magnitude* across training choices (e.g., 0.016 vs. 3375.355), underscoring substantial *measure fragility*.⁴

Takeaways. Under symmetry-preserving changes (FCN + same-permutation), a robust measure should not move; under signal destruction (independent permutations), it should reflect the loss of learnability. The PAC-Bayesian ML bound behaves in this manner in both architectures, whereas the path norm and PACBAYES-ORIG can vary dramatically with optimizer/stopping, masking the underlying data effect. Reporting such sensitivity is crucial when proposing or comparing generalization measures, in line with our paper’s emphasis on diagnosing and documenting *fragility*.⁴

H. Exp++ in scale-invariant nets: protocol and results

We instantiate the symmetry in a fully connected, *scale-invariant* network (normalization after each hidden linear layer; the final linear readout is frozen), trained on MNIST with SGD + momentum. We sweep a single control, the *Exp++ multiplicative factor* α from Theorem 6.2, which makes the learning rate grow exponentially across steps, and repeat the sweep both without and with weight decay. For each run we log parameter-space PAC–Bayes proxies (including magnitude-aware variants), path-norm proxies (with/without margin normalization), and test error. The stopping rule is cross-entropy unless stated otherwise.

Findings. Across both regimes (no WD and with WD) the test-error trace barely moves as α grows, yet the magnitude-sensitive diagnostics explode on a log scale. In particular, the PAC–Bayes family and the path-norm proxies rise by many orders of magnitude even though the error curve hugs a dashed 10% reference. This is exactly what the equivalence predicts in a scale-invariant net: Exp++ changes parameter *scale*, not the predictor—exposing the fragility of magnitude-dependent measures (notably PACBAYES-orig) in this setting.

⁴While label corruption is another standard knob for data complexity, here we focus on pixel permutations to isolate architectural symmetry vs. information destruction.

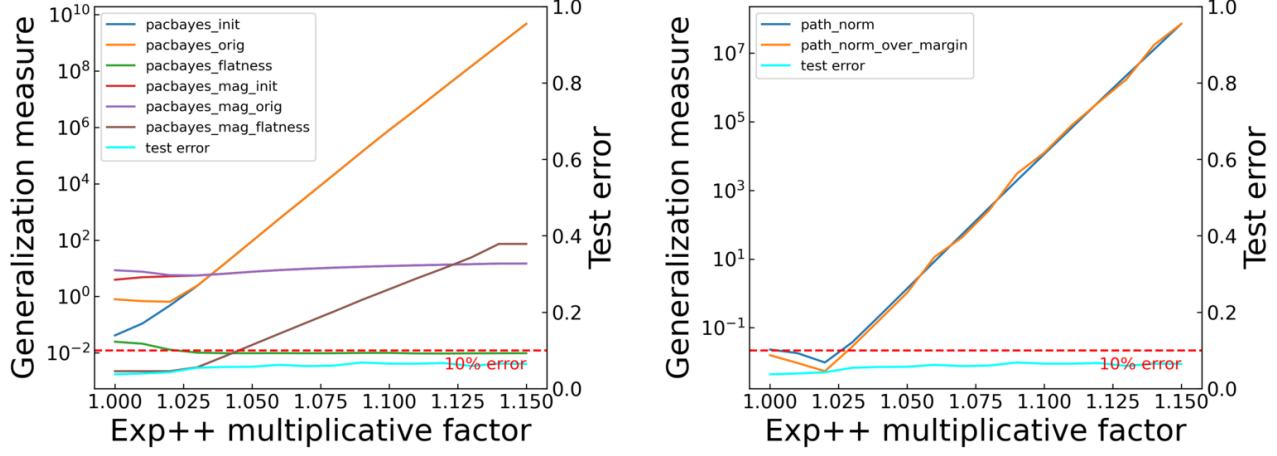


Figure S18. **Exp++ in a scale-invariant FCN (no WD; CE stopping).** As the Exp++ factor increases, PAC–Bayes proxies (left) and path-norm proxies (right) swell by orders of magnitude, while the test-error curve (right axis; dashed 10% line) remains essentially flat.

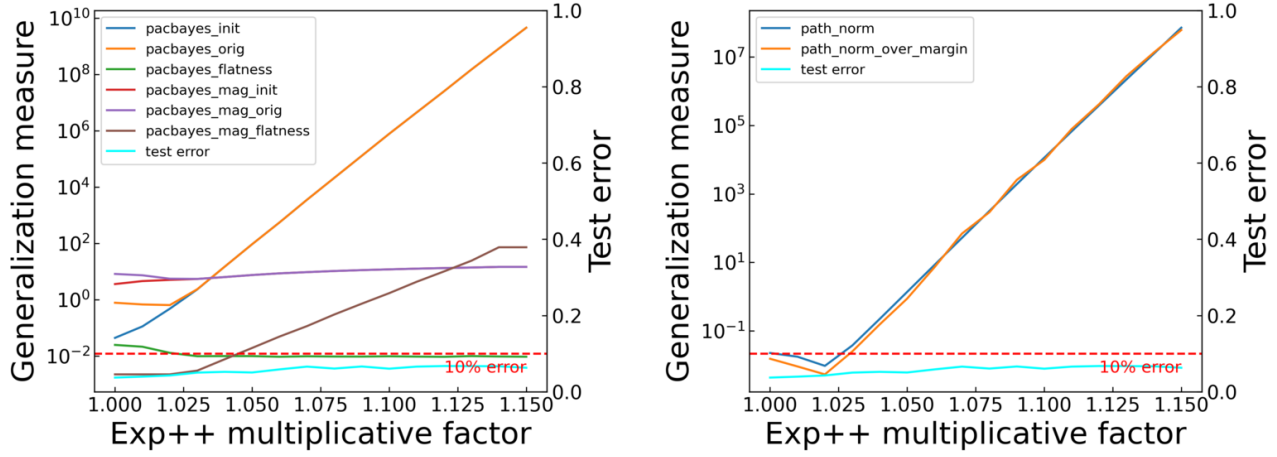


Figure S19. **Exp++ with weight decay (CE stopping).** The qualitative picture persists with WD: magnitude-sensitive PAC–Bayes and path-norm diagnostics climb sharply with the Exp++ factor, but the predictor’s test error barely changes.

Reading the panels. In both Figure S18 (no WD) and Figure S19 (with WD), left panels aggregate PAC–Bayes proxies; right panels show path-norm proxies. Axes are logarithmic for the measures and linear for the test error (right axis); the dashed horizontal line marks 10% test error for visual reference. Together, the panels illustrate a clean separation between *parameter scale* (which Exp++ manipulates) and *predictive behavior* (which stays essentially fixed).

Table 1. CMS and eCMS summary $\delta = 0.01$

Measure	CMS $_{\delta}^{\text{med}}$ /eCMS $_{\delta}^{\text{med}}$	C10/DN121	C10/NiN	C10/RN50	FMN/DN121	FMN/NiN	FMN/RN50
PARAMS	0.000 0.000 0.084 0.088 0.103 0.114 0.135 0.171 0.207 0.194 0.238 0.284 0.419 0.503 0.516 0.638 0.647 0.903 0.650 0.903 0.945 1.014 0.856 1.062 0.857 1.064 1.064 0.965 1.066 0.895 1.102 1.073 1.184 1.371 1.567 1.405 1.612 46.133 55.352 46.051 55.358 65.140 73.373 65.339 73.798 65.299 73.805 65.467 73.835	0.000 0.000 0.092 0.136 0.129 0.179 0.085 0.125 0.202 0.201 0.442 0.627 0.384 0.534 0.514 0.769 0.596 0.899 0.597 0.898 0.979 1.108 0.667 0.984 0.669 0.985 0.985 0.718 0.944 0.956 1.356 1.147 1.320 1.084 1.467 1.071 1.471 144.464 217.241 144.118 217.564 161.340 237.870 161.349 238.066 161.472 238.038 161.834 238.429	0.000 0.000 0.029 0.031 0.038 0.041 0.071 0.077 0.111 0.115 0.155 0.157 0.223 0.259 0.412 0.591 0.470 0.555 0.480 0.564 0.192 0.153 0.511 0.605 0.518 0.613 0.427 0.621 0.601 0.735 0.266 0.252 0.612 0.737 0.633 0.757 3.360 3.948 3.289 3.886 3.553 4.191 3.578 4.234 3.646 4.218 3.628 4.291	0.000 0.000 0.060 0.064 0.086 0.102 0.095 0.169 0.213 0.186 0.234 0.276 0.337 0.415 0.518 0.658 0.699 0.907 0.703 0.909 0.910 0.919 0.926 0.785 1.140 0.928 1.142 1.106 1.282 0.763 0.862 0.798 1.013 0.998 1.047 1.151 1.378 1.718 1.757 130.638 148.734 130.509 148.827 189.721 209.791 190.061 210.406 190.120 210.831 190.328 210.514	0.000 0.000 0.076 0.075 0.119 0.126 0.239 0.265 0.218 0.204 0.242 0.291 0.455 0.486 0.438 0.470 0.539 0.615 0.540 0.615 1.453 1.474 1.231 1.331 0.834 0.977 1.540 1.538 1.840 1.997 1.718 1.838 6.131 7.716 6.042 7.566 7.410 8.277 7.698 8.414 7.920 8.422 7.868 8.546	0.000 0.000 0.076 0.075 0.119 0.126 0.239 0.265 0.218 0.204 0.184 0.159 0.606 0.605 0.808 0.815 0.863 0.876 1.102 1.102 0.416 0.379 1.100 1.202 1.124 1.221 1.168 1.187 1.239 1.322 0.494 0.457 1.590 1.668 1.705 1.753 51.520 57.964 51.535 58.082 76.664 80.810 76.967 81.461 76.897 81.548 77.087 81.435	

Top numbers: CMS; bottom numbers: eCMS.

Table 2. CMS and eCMS summary $\delta = 0.02$

Measure	CMS $_{\delta}^{\text{med}}$ /eCMS $_{\delta}^{\text{med}}$	C10/DN121	C10/NiN	C10/RN50	FMN/DN121	FMN/NiN	FMN/RN50
PARAMS	0.000 0.000 0.094 0.095 0.118 0.139 0.165 0.183 0.227 0.204 0.244 0.253 0.486 0.535 0.557 0.697 0.695 0.872 0.694 0.872 0.872 1.023 1.008 0.882 1.040 0.884 1.041 1.041 0.960 1.064 1.052 1.105 1.158 1.182 1.482 1.629 1.537 1.666 45.667 52.105 45.569 52.134 66.789 72.385 67.284 72.701 67.196 72.740 67.235 SPEC.INIT.MAIN	0.000 0.000 0.106 0.137 0.139 0.170 0.100 0.126 0.224 0.205 0.470 0.597 0.431 0.516 0.581 0.761 0.657 0.868 0.656 0.869 0.869 1.037 1.043 0.735 0.961 0.734 0.961 1.033 1.318 0.818 0.947 1.208 1.268 1.227 1.452 1.221 1.434 159.109 210.065 158.752 210.292 177.665 232.486 177.627 232.516 177.751 232.603 177.757 232.667	0.000 0.000 0.046 0.047 0.049 0.047 0.088 0.090 0.122 0.114 0.190 0.188 0.328 0.337 0.768 0.797 0.648 0.797 0.646 0.791 0.252 0.204 0.772 0.891 0.774 0.961 0.935 1.014 0.850 0.959 0.349 0.323 0.998 1.117 1.052 1.156 4.538 5.582 4.520 5.538 5.294 6.130 5.420 6.298 5.401 6.235 5.432 6.237	0.000 0.000 0.064 0.068 0.097 0.108 0.092 0.135 0.247 0.219 0.261 0.283 0.352 0.398 0.533 0.644 0.733 0.875 0.733 0.875 1.009 0.973 0.952 1.120 0.956 0.900 0.822 0.988 0.777 0.846 1.107 1.096 1.190 1.117 1.124 1.156 42.519 50.772 42.487 50.732 55.105 64.848 55.458 64.973 55.227 64.942 55.198 64.927	0.000 0.000 0.107 0.114 0.173 0.174 0.270 0.292 0.230 0.232 0.228 0.224 0.542 0.553 0.438 0.437 0.534 0.586 0.533 0.586 1.928 1.891 0.811 0.870 0.813 0.870 0.781 0.928 1.438 1.504 1.914 1.874 2.132 2.225 1.973 2.061 129.111 141.794 129.093 141.846 195.785 209.989 196.634 210.576 196.343 210.513 197.145 210.896	0.000 0.000 0.082 0.079 0.072 0.068 0.230 0.232 0.251 0.128 0.170 0.143 0.746 0.731 0.755 0.749 0.930 0.842 0.913 1.076 0.582 0.546 1.162 1.221 1.182 1.240 1.282 1.323 1.254 1.250 0.623 0.580 1.738 1.806 1.853 1.899 6.510 7.677 6.391 7.530 7.909 8.296 8.272 8.678 8.133 8.548 8.288 8.751	0.000 0.000 0.110 0.111 0.199 0.187 0.410 0.419 0.218 0.413 0.401 0.607 0.603 0.503 0.490 0.842 0.921 0.839 0.923 2.083 2.017 1.365 1.389 1.364 1.387 0.985 1.114 1.390 1.394 2.116 2.086 2.042 2.061 2.043 2.058 48.816 53.437 48.650 53.537 78.473 79.923 79.109 80.429 79.165 80.539 79.271 80.867

Top numbers: CMS; bottom numbers: eCMS.

Table 3. CMS and eCMS summary $\delta = 0.05$

Measure	CMS $_{\delta}^{\text{med}}$ /eCMS $_{\delta}^{\text{med}}$	C10/DN121	C10/NiN	C10/RN50	FMN/DN121	FMN/NiN	FMN/RN50
PARAMS	0.000 0.000 0.096 0.096 0.136 0.144 0.188 0.198 0.246 0.210 0.299 0.311 0.627 0.628 0.558 0.665 0.781 0.862 0.785 0.867 0.955 1.097 1.288 1.218 1.115 1.235 1.124 1.245 1.241 1.254 1.367 1.296 1.659 1.708 1.763 1.807 45.293 50.008 45.538 50.283 73.068 78.684 73.576 79.426 73.690 79.493 73.884 SPEC.INIT.MAIN	0.000 0.000 0.117 0.131 0.133 0.143 0.138 0.162 0.228 0.191 0.395 0.442 0.448 0.478 0.550 0.655 0.622 0.757 0.623 0.757 0.985 1.164 1.220 1.134 0.744 0.856 0.744 0.857 0.973 1.012 1.322 1.242 1.442 1.561 1.387 1.453 150.478 183.171 150.676 183.231 179.892 206.998 180.133 207.233 180.019 207.366 180.209 207.184	0.000 0.000 0.056 0.054 0.067 0.064 0.143 0.143 0.167 0.155 0.221 0.204 0.539 0.540 0.972 0.989 1.033 1.132 1.045 1.141 1.359 1.445 0.445 0.403 1.216 1.252 1.227 1.269 1.227 1.253 1.257 1.322 1.242 1.578 1.605 1.670 1.713	0.000 0.000 0.075 0.076 0.139 0.145 0.095 0.111 0.265 0.229 0.310 0.347 0.392 0.426 0.566 0.676 0.763 0.917 0.765 0.918 0.854 1.030 1.356 1.303 1.069 1.251 1.068 1.269 1.257 1.413 0.556 0.520 1.349 1.605 1.670 1.713	0.000 0.000 0.110 0.113 0.286 0.289 0.369 0.389 0.323 0.297 0.288 0.275 0.715 0.717 0.473 0.461 0.498 0.545 0.501 0.547 0.702 0.774 3.325 3.351 0.819 0.845 0.819 0.848 1.777 1.803 3.133 3.149 2.577 2.656 2.500 2.535 120.482 131.962 121.211 132.342 197.573 204.030 198.114 204.537 198.217 205.168 199.461 206.594	0.000 0.000 0.082 0.079 0.073 0.068 0.233 0.234 0.145 0.127 0.170 0.141 0.754 0.738 0.751 0.744 0.911 1.070 0.929 1.090 1.281 1.321 0.593 0.555 1.161 1.219 1.180 1.238 1.256 1.251 1.251 1.632 0.590 1.740 1.810 1.856 1.901 6.377 7.487 6.503 7.627 7.901 8.281 8.128 8.533 8.533 8.262 8.664 8.284 8.740	0.000 0.000 0.120 0.119 0.302 0.290 0.561 0.569 0.364 0.326 0.411 0.381 0.796 0.782 0.505 0.470 0.799 0.807 0.805 0.816 0.925 0.975 4.025 4.024 1.468 1.488 1.473 1.489 1.864 1.849 3.930 3.921 2.778 2.777 2.646 2.653 46.334 46.814 46.690 47.308 84.367 85.503 85.126 86.313 85.409 86.340 85.783 86.990

Top numbers: CMS; bottom numbers: eCMS.

Table 4. Pixel permutations with **MNIST + FCN** (training set size $n=10,000$). Same-permutation preserves the FCN's permutation symmetry; independent (random) permutations destroy learnable signal.

Optimizer / stopping	Test err.	PAC-Bayes ML	Path norm	PACBAYES-ORIG
<i>Unshuffled pixels</i>				
SGD / CE	0.033	0.142	0.080	1.534
ADAM / CE	0.034	0.142	0.173	1.208
SGD / Acc	0.032	0.142	0.081	1.535
ADAM / Acc	0.031	0.142	0.379	1.187
<i>Same permutation on train & test</i>				
SGD / CE	0.032	0.142	0.080	1.558
ADAM / CE	0.034	0.142	0.184	1.202
SGD / Acc	0.032	0.142	0.081	1.534
ADAM / Acc	0.032	0.142	0.314	1.183
<i>Independent random permutations (train & test)</i>				
SGD / CE	0.497	0.532	0.124	2.232
ADAM / CE	0.492	0.532	5.736	1.791
SGD / Acc	0.498	0.532	0.105	2.400
ADAM / Acc	0.488	0.532	6.632	1.837

CE: best checkpoint by cross-entropy; Acc: best checkpoint by accuracy.

Table 5. Pixel permutations with **MNIST + ResNet-50** ($n=10,000$). Convolutional inductive biases depend on spatial locality, so even a single shared permutation harms performance.

Optimizer / stopping	Test err.	PAC-Bayes ML	Path norm	PACBAYES-ORIG
<i>Unshuffled pixels</i>				
SGD / CE	0.022	0.101	2980.415	15.396
ADAM / CE	0.016	0.101	0.173	4.498
SGD / Acc	0.025	0.101	2972.887	15.125
ADAM / Acc	0.014	0.101	0.022	4.417
<i>Same permutation on train & test</i>				
SGD / CE	0.060	0.170	3375.355	13.534
ADAM / CE	0.046	0.170	0.016	4.074
SGD / Acc	0.056	0.170	3001.528	12.529
ADAM / Acc	0.041	0.170	0.021	3.909
<i>Independent random permutations (train & test)</i>				
SGD / CE	0.460	0.504	116.602	13.77
ADAM / CE	0.437	0.504	0.081	4.157
SGD / Acc	0.460	0.504	67.497	12.475
ADAM / Acc	0.437	0.504	0.084	4.119

CE: best checkpoint by cross-entropy; Acc: best checkpoint by accuracy.